

DOE-R-71-2570

DOE-R-71-2570  
distribution public release  
distribution unlimited

DOE-R-71-2570  
30620

# Shock Dynamics Laboratory

## Department of Physics



# Washington State University

Pullman, Washington 99164

Reproduced by  
**NATIONAL TECHNICAL  
INFORMATION SERVICE**  
Springfield, Va. 22151

122

Unclassified

Security Classification

DOCUMENT CONTROL DATA - R & D

(Security classification of title, body of abstract and indexing information must be entered when the overall report is classified)

1. ORIGINATING ACTIVITY (Corporate author)

Department of Physics  
Washington State University  
Pullman, Wa. 99163

2a. REPORT SECURITY CLASSIFICATION

Unclassified

2b. GROUP

3. REPORT TITLE

SHOCK INDUCED MAGNETIC ANISOTROPY IN YTTRIUM IRON GARNET

4. DESCRIPTIVE NOTES (Type of report and inclusive dates)

Scientific--Interim

5. AUTHOR(S) (First name, middle initial, last name)

Dennis E. Grady

6. REPORT DATE

August 1971

7a. TOTAL NO. OF PAGES

120

7c. NO. OF REFS

64

8a. CONTRACT OR GRANT NO.

AFOSR 69-1758

9a. ORIGINATOR'S REPORT NUMBER(S)

b. PROJECT NO.

9761-01

9b. OTHER REPORT NO(S) (Any other numbers that may be assigned this report)

c.

681301

AFOSR - TR - 71-2570

d.

10. DISTRIBUTION STATEMENT

Approved for public release;  
distribution unlimited.

11. SUPPLEMENTARY NOTES

TECH, OTHER

12. SPONSORING MILITARY ACTIVITY

Air Force Office of Scientific Research  
(NE) 1400 Wilson Blvd.  
Arlington, Va. 22209

13. ABSTRACT Shock induced demagnetization produced by strain induced magnetic anisotropy is considered in single crystal and polycrystalline ferromagnetic material. A consistent application of equilibrium thermodynamics in conjunction with established tools of ferromagnetic domain theory is used to develop energy expressions, magnetization curves, and domain structure in the magnetic material behind the shock wave. This approach has not previously been used to describe the shock induced anisotropy effect. In particular, specific expressions for the exchange energy and magnetic self energy are explicitly obtained. They are predicted to increase as the fourth root of the strain and are small compared to the induced anisotropy energy in the region of large elastic and plastic strain. A needle or sliver shaped domain structure oriented in the direction of shock propagation is expected to nucleate behind the shock front. These results follow from the domain theory analysis and have not previously been obtained.

In polycrystalline material, the averaging procedure required to predict the magnetic behavior is critically analyzed. The importance of magnetic grain-grain interaction is pointed out and magnetization curves for the extreme assumptions of interacting grains and independent grains are determined. The effect of porosity and finite strain is also considered. These results are compared with those obtained by Shaner and Royce (J. Appl. Phys. 39, 492 (1968)) for interacting grains and effects of finite strain.

Experimental demagnetization curves are obtained for shocked polycrystalline yttrium iron garnet at about one-third and two-thirds the Hugoniot elastic limit of the material. The results support the independent grain theory.

DD FORM NOV 65 1473

CONTINUED-----

Security Classification

## DOCUMENT CONTROL DATA - R &amp; D

(Classification of title, body of abstract and indexing annotation must be entered when the overall report is classified)

NG ACTIVITY (Corporate author)

2a. REPORT SECURITY CLASSIFICATION

2b. GROUP

page 2 -- continued

REPORT TITLE

## 4. DESCRIPTIVE NOTES (Type of report and inclusive dates)

## 5. AUTHOR(S) (First name, middle initial, last name)

6. REPORT DATE

7a. TOTAL NO. OF PAGES

7b. NO. OF REFS

8a. CONTRACT OR GRANT NO.

9a. ORIGINATOR'S REPORT NUMBER(S)

b. PROJECT NO.

c.

d.

9b. OTHER REPORT NO(S) (Any other numbers that may be assigned this report)

## 10. DISTRIBUTION STATEMENT

## 11. SUPPLEMENTARY NOTES

## 12. SPONSORING MILITARY ACTIVITY

## 13. ABSTRACT

continued---

During this work a successful experimental technique was developed which, in conjunction with a gas gun used for impact studies, applies the required uniaxial strain field and magnetic field and measures the subsequent shock induced demagnetization.

DD FORM 1 NOV 65 1473

Security Classification

Approved for public release:  
distribution unlimited.

SHOCK INDUCED MAGNETIC ANISOTROPY IN YTTRIUM IRON GARNET

Dennis E. Grady

WSU SDL 71-03

August 1971

This work was submitted in partial fulfillment of the requirements of the Ph.D. degree in Physics, Washington State University. It was supported by the Air Force Office of Scientific Research, under Grant No. AFOSR 69-1758.

## ABSTRACT

Shock induced demagnetization produced by strain induced magnetic anisotropy is considered in single crystal and polycrystalline ferromagnetic material. A consistent application of equilibrium thermodynamics in conjunction with established tools of ferromagnetic domain theory is used to develop energy expressions, magnetization curves, and domain structure in the magnetic material behind the shock wave. This approach has not previously been used to describe the shock induced anisotropy effect. In particular, specific expressions for the exchange energy and magnetic self energy are explicitly obtained. They are predicted to increase as the fourth root of the strain and are small compared to the induced anisotropy energy in the region of large elastic and plastic strain. A needle or sliver shaped domain structure oriented in the direction of shock propagation is expected to nucleate behind the shock front. These results follow from the domain theory analysis and have not previously been obtained.

In polycrystalline material, the averaging procedure required to predict the magnetic behavior is critically analyzed. The importance of magnetic grain-grain interaction is pointed out and magnetization curves for the extreme assumptions of interacting grains and independent grains are determined. The effect of porosity and finite strain is also considered. These results are compared with those obtained by Shaner and Royce (J. Appl. Phys. 39, 492 (1968)) for interacting grains and effects of finite strain.

Experimental demagnetization curves are obtained for shocked polycrystalline yttrium iron garnet at about one-third and two-thirds the Hugoniot elastic limit of the material. The results support the independent grain theory.

During this work a successful experimental technique was developed which, in conjunction with a gas gun used for impact studies, applies the required uniaxial strain field and magnetic field and measures the subsequent shock induced demagnetization.

## TABLE OF CONTENTS

	Page
<b>ABSTRACT . . . . .</b>	<b>ii</b>
<b>Chapter</b>	
<b>I. INTRODUCTION . . . . .</b>	<b>1</b>
1.1. Background . . . . .	1
1.2. Objectives . . . . .	2
<b>II. THERMODYNAMICS OF THE ANISOTROPIC FERROMAGNET . . . . .</b>	<b>4</b>
2.1. Magnetic Work . . . . .	5
2.2. Thermodynamic Laws . . . . .	9
2.3. The Local Energy . . . . .	10
2.4. Phenomenological Expression . . . . .	15
<b>III. APPLICATION TO THE SHOCK INDUCED ANISOTROPY EFFECT . . . . .</b>	<b>20</b>
3.1. Domain Theoretical Calculation (Single Crystal) . . . . .	22
3.1.1. Induced Anisotropy Energy . . . . .	24
3.1.2. Exchange Energy . . . . .	26
3.1.3. Demagnetizing Energy. . . . .	30
3.1.4. Total Energy . . . . .	30
3.2. Domain Theoretical Calculation (Polycrystal) . . . . .	33
3.2.1. Interacting Grain Assumption . . . . .	34
3.2.2. Independent Grain Assumption . . . . .	38
3.3. Micromagnetic Theory . . . . .	42
3.4. Porosity Effect . . . . .	44
<b>IV. EXPERIMENTAL METHOD. . . . .</b>	<b>49</b>
4.1. Application of Magnetic Field. . . . .	51
4.2. Application of Strain Field. . . . .	55
4.2.1. Experimental Construction . . . . .	55

	Page
4.2.2. Equation of State . . . . .	58
4.3. Demagnetization Measurement . . . . .	61
4.4. Material . . . . .	64
4.5. Experimental Corrections . . . . .	68
V. ANALYSIS OF EXPERIMENTAL DATA . . . . .	74
5.1. Magnetic Field . . . . .	74
5.2. Uniaxial Strain Field . . . . .	75
5.3. Transverse Magnetization . . . . .	77
5.4. Experimental Data . . . . .	81
VI. DISCUSSION AND CONCLUSIONS . . . . .	87
6.1. Discussion . . . . .	87
6.2. Summary . . . . .	91
REFERENCES . . . . .	92
APPENDIX	
I. TABLE OF THERMODYNAMIC AND ENERGY EXPRESSIONS . . . . .	96
II. LIST OF SYMBOLS . . . . .	98
III. FINITE STRAIN EFFECT . . . . .	101
III.1. The Finite Strain Tensor . . . . .	101
III.2. Finite Strain Correction to Interacting Grain Theory . . . . .	102
III.3. Finite Strain Correction to Independent Grain Theory . . . . .	105
IV. MAGNETOELASTIC ENERGY ABOUT A SPHERICAL PORE . . . . .	108
V. DEVIATION FROM UNIFORM STRAIN . . . . .	112

## CHAPTER I

### INTRODUCTION

Creation of an anisotropic ferromagnet by subjecting a ferromagnetic material to a planar shock wave produces the shock induced magnetic anisotropy effect. The resulting uniaxial strain establishes a magnetic anisotropy field which fundamentally affects the magnetic behavior of the material. A quantitative understanding of this shock induced magnetic behavior is necessary before a complete description of the response of magnetic materials to dynamic loading can be determined.

#### 1.1 Background

The interdependence of magnetic and elastic behavior of ferromagnetic material was first established by Joule<sup>1</sup> in 1842 when he observed the change in length of a ferromagnetic bar upon magnetization. The inverse effect (Villari effect) or the change in magnetization with applied tension was reported in 1865.<sup>2</sup> There followed a rash of discoveries of magnetostrictive effects and related inverse effects which were finally incorporated into a coherent theory with the advent of conventional magnetoelastic theory in the early 1930's.<sup>3</sup> Intensive research in the 1940's and 1950's established the foundations of domain theory.<sup>4</sup> Finally, a consistent thermodynamic treatment of magnetoelastic interactions by Brown<sup>5</sup> (1963) refined the conventional theory to its fairly sound foundation of the present day.

The shock induced anisotropy effect is a specific form of the general piezomagnetic or inverse magnetostriction effect. Its contribution to the

shock induced demagnetization problem was established by Royce<sup>6</sup> (1966) while investigating the magnetic response of nickel ferrite under shock loading. Subsequent work by Royce<sup>7</sup> and Shaner and Royce<sup>8</sup> in the plastic region of yttrium iron garnet and Seay et al.<sup>9</sup> in the elastic and plastic regions of manganese zinc ferrite confirmed this conclusion. The effect in single crystal and polycrystal ferrites has been considered theoretically by Bartel.<sup>10,11</sup> Wayne, Samara, and Lefever<sup>12</sup> have observed a form of this effect which occurs locally in porous ferromagnetic material subject to hydrostatic pressure.

There has been continuing interest in this magnetic effect peculiar to the realm of shock wave physics. The interest has recently been increased by attempts to understand the magnetic response of natural and meteoritic material under dynamic loading. This understanding is necessary to be confident in using magnetic techniques for investigation of the history and origin of such materials.

### 1.2. Objectives

The work cited in the previous section represents a significant contribution to the definition and understanding of the shock induced anisotropy effect. However, it is the belief of this author that the extension of this understanding to the prediction of the magnetic response of actual material subject to shock loading requires a firmer quantitative foundation than is now available. The intention of this work is to contribute theoretical and experimental groundwork toward this foundation.

The objectives undertaken in this work are as follows: The necessary thermodynamics for a systematic description of the induced anisotropic ferromagnet will be developed. The shock induced anisotropy effect in single

crystal ferromagnetic material will be considered by a consistent application of the established tools of domain theory; In particular, the contributions of the exchange energy and demagnetizing energy will be determined. The domain structure behind the shock wave will be deduced from this domain theoretical analysis. Following this, the shock induced anisotropy effect in polycrystalline ferromagnetic material will be considered. Integral in this consideration is a critical analysis of the averaging process required to predict the random behavior of the polycrystalline structure. The contribution due to finite strain, a serious question in the region of large elastic strain, will be determined. Finally, the effect of porosity on the macroscopic magnetic response of material subject to this effect will be addressed.

Further objectives of this work are the design and implementation of an experimental technique capable of measuring the magnetic state of the shocked ferromagnetic material during the few tenths of a microsecond within which this state exists. With this method data is accumulated in the region of large elastic strain in yttrium iron garnet. Favorable magnetic properties of yttrium iron garnet provide a critical comparison of experiment with theory.

## CHAPTER II

### THERMODYNAMICS OF THE ANISOTROPIC FERROMAGNET

The effect of propagating a one dimensional shock wave through a ferromagnetic material is to create a state of uniform uniaxial strain behind the shock wave. This allows use of the thermodynamics of rigid ferromagnets<sup>5</sup> in this region. This thermodynamic state is maintained by the inertial characteristics of the material and is difficult to obtain by means other than shock wave techniques. It will persist until perturbing waves subject the region to further change. The goal is to predict the magnetic behavior in the shocked region while it is still in a state of uniaxial strain.

The intent of this chapter is to develop consistently the thermodynamics necessary to describe an anisotropic ferromagnet<sup>5</sup> and to obtain the magnetic work term along with the appropriate thermodynamic equilibrium and stability criteria. A complete phenomenological energy expression will be constructed.

This chapter contains nothing that is not already in the literature. It represents a survey, from many sources, for a complete thermodynamic description of the shock induced anisotropy effect. Its content is not necessary for an understanding of the remaining chapters. The various thermodynamic terms and expressions derived in this chapter and used throughout the text have been collected in Appendix I for easy reference.

A thermodynamic approach through an energy expression rather than through direct consideration of the forces involved will be used for several

reasons. First, a phenomenological approach relating the forces directly requires a stress hypothesis. Inherent in the stress formulation is a non-uniqueness in that any second rank tensor with zero divergence can be added to the stress tensor without affecting the equations of motion or the boundary conditions. This is usually of little consequence. In magnetic material, however, there is an additional complication to the nonuniqueness. This arises in attempting to separate short range magnetic forces, which will contribute to the stress, from long range magnetic forces, which will contribute to the volume force. A magnetic pole formalism, an Amperian current formalism, or any of several others gives different separation of magnetic stresses and magnetic volume forces.<sup>5</sup> In a thermodynamic consideration, the energy expression is unique and these complicating problems are avoided. Second, when forces are considered directly stability is checked only with difficulty. In thermodynamics stability emerges naturally and simply in the second variation of the energy expression.<sup>13</sup>

### 2.1. Magnetic Work

The magnetic work done on a magnetic system can be obtained by considering the work done by a source of emf and the related change in magnetic flux through Faraday's law. Alternately, one can obtain the same expression from Maxwell's equations by somewhat more laborious methods. The two are, of course, equivalent. The latter method will be used since this is the point at which most electromagnetic texts prematurely terminate. Also, this method more clearly shows the points at which deviation from complete generality occurs.

The work expression

$$\delta W = \frac{1}{4\pi} \int \vec{H} \cdot \vec{\delta B} dV + \frac{1}{4\pi} \int \vec{E} \cdot \vec{\delta D} dV + \int \vec{J} \cdot \vec{\delta t} dV \quad (2.1)$$

is obtained directly from Maxwell's equations.<sup>14</sup> Gaussian units are used and  $\vec{H}$ ,  $\vec{B}$ ,  $\vec{E}$ ,  $\vec{D}$ , and  $\vec{J}$  are the usual field quantities of electromagnetic theory. This expression assumes only that current changes are sufficiently quasistatic so that negligible energy is lost from the system by radiation. Nothing is assumed about linearity, reversibility, etc. in the magnetic material. The three terms are, respectively, the magnetic work, the electric work, and the work done in creating Joule heat by the true currents in the system. If the ferromagnet is nonconductive and incapable of storing electric energy, then only the first term

$$\delta W = \frac{1}{4\pi} \int \vec{H} \cdot \delta \vec{B} dV \quad (2.2)$$

is important.

The work done on the ferromagnet is stored in various forms of energy or dissipated in irreversible processes. The work expression in this form does not show this partitioning. To proceed further, the magnetic field intensity will be separated into two fields,

$$\vec{H} = \vec{H}_e + \vec{H}_d. \quad (2.3)$$

This is possible through a theorem due to Helmholtz.<sup>15</sup>  $\vec{H}_e$  is solenoidal and is the particular solution of the equation

$$\vec{\nabla} \times \vec{H}_e = \frac{4\pi}{c} \vec{J}$$

and  $\vec{H}_d$  is irrotational and is the particular solution of the equation

$$\vec{\nabla} \cdot \vec{H}_d = -4\pi \vec{\nabla} \cdot \vec{M}.$$

In other words,  $\vec{H}_e$  has as sources current carrying conductors such as would

be used to magnetize the magnetic material and will hereafter be called the external field.  $\vec{H}_d$  has as sources surface and volume magnetic poles and will be called the demagnetizing or dipolar field. It should be remembered that an entirely equivalent partitioning can be done with the magnetic induction  $\vec{B}$ . The development would then evolve around the concept of free currents and Amperian currents. Although either method is acceptable, the first is commonly used since it allows greater mathematical simplicity and some physical insight depending on one's prejudices on magnetic pole concepts.

With this separation of the magnetic field intensity and with

$$\delta\vec{B} = \delta\vec{H} + 4\pi\delta\vec{M},$$

Equation (2.2) becomes

$$\delta W = \int \left[ \vec{H} \cdot \delta\vec{M} + \frac{\vec{H}_e^2}{8\pi} + \frac{\vec{H}_d^2}{8\pi} + \frac{\vec{H}_e \cdot \vec{H}_d}{4\pi} \right] dV.$$

In the last term,  $\vec{H}_d$  is irrotational and can be written as the gradient of a scalar potential,  $\phi_m$ . Integration by parts produces two terms. One contains  $\vec{\nabla} \cdot \vec{H}_e$  and is, therefore, zero and the other contains the total divergence of  $\phi_m \vec{H}_e$  and, therefore, transforms to a surface integral. Assuming the system is localized so that  $r_{\phi_m}$  and  $r^2 H_e$  are regular at infinity demands that the integrand diminishes sufficiently fast so that the surface integral must vanish. The other terms can be identified. The second term is the work done in changing the external field energy and does not depend on the magnetic material. This term will be excluded from thermodynamic consideration of the ferromagnet. It is entirely a matter of bookkeeping and does not create any problems.<sup>16</sup> The third term is the magnetostatic "self energy" of the ferromagnet. It represents the energy required to

construct the distribution of magnetic dipoles in the ferromagnet against the dipole-dipole, "action at a distance" forces. This term differs from the dipole-dipole energy only by the volume integral of a term which depends on local conditions in the magnetic material and may be regarded as an energy density.<sup>5</sup> The first term is either the work done in storing energy in local form (expressible as a volume integral of an energy density) or the work lost in irreversible processes.

The final magnetic work is

$$\delta W = \int \vec{H} \cdot \vec{\delta M} \, dV + \delta \int \frac{H_d^2}{8\pi} \, dV. \quad (2.4)$$

Using two well known theorems from magnetostatics,<sup>17</sup>

$$\int \vec{H}_d \cdot \vec{B}_d \, dV = 0$$

and

$$\int \vec{H}_d \cdot \vec{\delta M} \, dV = \int \vec{M} \cdot \vec{\delta H}_d \, dV,$$

the following useful forms for the magnetic work can be obtained

$$\delta W = \int \vec{H} \cdot \vec{\delta M} \, dV - \frac{1}{2} \delta \int \vec{H}_d \cdot \vec{M} \, dV \quad (2.5)$$

or

$$\delta W = \int \vec{H}_e \cdot \vec{\delta M} \, dV. \quad (2.6)$$

The latter is the form obtained directly from a consideration of Faraday's law relating the emf to the flux change.<sup>5</sup>

## 2.2. Thermodynamic Laws

The combined first and second law of thermodynamics states that

$$\delta U \leq T\delta S + \int \vec{H}_e \cdot \vec{\delta M} dV$$

in a natural process.<sup>13</sup> For a ferromagnet constrained to  $S = S_0$  and  $\vec{M} = \vec{M}_0$ , this is

$$\delta U \leq 0.$$

The internal energy can only decrease. This law implies that a virtual variation of the energy with respect to internal coordinates must be zero (thermodynamic equilibrium) and that this energy be already as small as possible (thermodynamic stability).

The constraint on the magnetization is difficult to realize experimentally. The controllable parameter is the external magnetic field,  $\vec{H}_e$ . The usual thermodynamic technique is to perform an appropriate Legendre transformation to an energy function with the controllable parameters as independent variables.<sup>13</sup> The energy function to be used will be

$$E = U - \int \vec{H}_e \cdot \vec{M} dV$$

and will be referred to simply as the energy.

$$\delta E = \delta U - \int \vec{M} \cdot \vec{\delta H}_e dV - \int \vec{H}_e \cdot \vec{\delta M} dV$$

With the combined first and second law, this becomes

$$\delta E \leq T\delta S - \int \vec{M} \cdot \vec{\delta H}_e dV.$$

For a ferromagnet constrained to  $S = S_0$  and  $\vec{H}_e = \vec{H}_{e0}$ ,

$$\delta E \leq 0,$$

and the thermodynamic equilibrium and stability criteria in terms of this energy are evident.

### 2.3. The Local Energy

It is the intent of this development to use the energy

$$E = U - \int \vec{H}_e \cdot \vec{M} dV \quad (2.7)$$

along with the thermodynamic equilibrium and stability criteria to predict equilibrium states for a rigid anisotropic ferromagnet. To do this, an explicit expression for  $U$  in terms of pertinent internal coordinates must be obtained.  $U$  can be written

$$U = E_D + \int \epsilon_{LOC} dV \quad (2.8)$$

where  $E_D$  is either of the previously derived self energy expressions in Equation (2.4) or Equation (2.5). The remaining energy depends only on local conditions and can be written as the volume integral of an energy density.

It is this term that is now of concern.

The method used to obtain this local energy expression is to rely on physics and microscopic models of the magnetic material to guide in the selection of mathematical forms and independent variables for the local energy. Phenomenological methods such as convenient expansions and symmetry requirements are then used to deduce precise forms for the energy expression.<sup>5</sup>

The dominant local energies in a ferromagnet have been classified as the exchange energy, the magnetocrystalline anisotropy energy, the magnetoelastic energy, and the elastic energy.<sup>4</sup> Each will be considered in order.

The exchange energy has a purely quantum mechanical origin. It can be traced to the requirement of antisymmetry of the electronic state of the

magnetic ions under interchange of any two electrons.<sup>18</sup> In considering the interaction of any two magnetic ions, the antisymmetry requirement produces a splitting of energy levels making parallel and antiparallel spin alignment energetically separate. In a magnetic material at normal temperatures, only the lower lying energy states will be abundantly populated so the complete Hamiltonian may be replaced by an "effective spin Hamiltonian" which has as its energy eigenvalues these several low lying states.<sup>19</sup> Between any two magnetic ions, this effective spin Hamiltonian can be written as

$$\mathcal{H}_s = -2J_{ij}\vec{S}_i \cdot \vec{S}_j.$$

$J_{ij}$  is the exchange integral which determines the splitting of the low lying states.<sup>20</sup> If  $J_{ij}$  is a positive quantity, parallel spin is a lower energy state and ferromagnetism results. For  $J_{ij}$  negative, antiparallel spin is a lower energy state and antiferromagnetism results. The Hamiltonian for the entire crystal is

$$\mathcal{H}_s = -2 \sum_{ij} J_{ij}\vec{S}_i \cdot \vec{S}_j.$$

This exchange energy gives rise to a very strong but short range interaction causing a cooperative alignment of magnetic dipoles and hence a spontaneous macroscopic magnetization in the material. The magnitude of this magnetization has been found, with few exceptions, to be isotropic<sup>21</sup> and to depend mainly on the temperature<sup>22</sup> and to some extent on the pressure in the medium.<sup>23</sup> The small pressure dependence is considered in Section 4.5 To make an adequate selection of thermodynamic variables upon which the macroscopic expression for the exchange energy will depend, one can look to the result of a simple model. The following model will suggest that the gradients of the components of the magnetization or, alternatively, the gradients of the

direction cosines will be the proper thermodynamic variables.<sup>22</sup> Consider a simple cubic ferromagnetic material in which the exchange integral is isotropic.

$$\mathcal{H}_s = -2J \sum_{ij} \vec{s}_i \cdot \vec{s}_j$$

If the spin directions change gradually so that adjacent spins differ by small angles, the quantum spin operators may be replaced by classical angular momentum vectors.

$$E = -2JS^2 \sum_{ij} \vec{\alpha}_i \cdot \vec{\alpha}_j$$

where  $\vec{\alpha}_j$  is a unit vector in the direction of spin j.

$$\vec{\alpha}_i \cdot \vec{\alpha}_j = \cos \phi_{ij}$$

may be expanded giving

$$E = -2JS^2 \sum_{ij} \left(1 - \frac{1}{2}(\vec{\alpha}_i - \vec{\alpha}_j)^2\right)$$

$$\approx -2JS^2 \sum_{ij} \left(1 - \frac{1}{2}(r_{ij} \nabla \alpha)^2\right),$$

where  $\vec{r}_{ij}$  is a vector between magnetic ions having spin  $\vec{s}_i$  and  $\vec{s}_j$  and  $\vec{\alpha}_i$  is extended to a continuous function of position. If only nearest neighbor interactions are assumed and the sum is extended over six nearest neighbors,

$$E \approx -2JS^2 \sum_i \left\{ 6 - a^2 \left[ \left( \frac{\partial \vec{\alpha}}{\partial x} \right)^2 + \left( \frac{\partial \vec{\alpha}}{\partial y} \right)^2 + \left( \frac{\partial \vec{\alpha}}{\partial z} \right)^2 \right] \right\}.$$

Other terms in the sum are zero because of cubic symmetry. Dropping the constant term and allowing  $N$  magnetic atoms per unit volume, the energy density becomes

$$\epsilon_{ex} = 2JS^2a^2N \left[ \left( \frac{\partial \vec{a}}{\partial x} \right)^2 + \left( \frac{\partial \vec{a}}{\partial y} \right)^2 + \left( \frac{\partial \vec{a}}{\partial z} \right)^2 \right].$$

This suggests that in more general cases the functional dependence of the exchange energy will be

$$\epsilon_{ex} \left( \frac{\partial \vec{a}}{\partial x}, \frac{\partial \vec{a}}{\partial y}, \frac{\partial \vec{a}}{\partial z} \right).$$

In ferrimagnetic materials, which include spinel structures such as nickel ferrite and manganese zinc ferrite and garnet structures such as yttrium iron garnet, this exchange phenomenon becomes somewhat more complicated. The complication arises from the existence of diamagnetic cations regularly dispersed throughout the lattice. The exchange interaction between magnetic anions is coupled through these diamagnetic cations. Due to the large separation of the magnetic ions, there is smaller overlap of state functions and the exchange integral is negative. This type of exchange exhibited in ferrimagnetic materials is called superexchange and results in an antiferromagnetic alignment of electron spins.<sup>24</sup> It is found, however, that, as in the ferromagnetic case, the total Hamiltonian can again be conveniently replaced by an effective spin Hamiltonian. But, each different magnetic sublattice must be treated separately. We may still expect that a macroscopic expression for the exchange energy will be functionally dependent on the magnetization gradients.

It is observed in ferromagnetic materials that under zero applied field magnetic domains lie along preferred crystal directions.<sup>25</sup> Work must

be done on the system to rotate magnetic domains out of these directions. The local energy term associated with this interaction has been named the magneto-crystalline anisotropy energy. It has been observed that this energy term does not affect the magnitude of the saturation magnetization and depends only on the direction of the saturation magnetization relative to the local crystallographic axis.<sup>26</sup> This is a consequence of the fact that the exchange energy is much larger than the anisotropy energy and depends on the inner product of spin operators which are isotropic. Microscopically, the dominant contributing interaction to this energy is through single ion interaction with the crystal lattice.<sup>26</sup> The spin-orbit coupling prefers a colinear alignment of electron spin and orbital angular momentum while the orbital charge cloud adjusts itself in the crystal field to minimize electrostatic energy. Thus, the spin magnetic moment sees the crystal lattice through the spin orbit coupling.

The magnetoelastic energy has the same origin as the magnetocrystalline anisotropy energy. It is a consequence of the fact that the anisotropy energy is dependent on the lattice dimensions. To distort the crystal lattice in any way may change the anisotropy energy. This energy deviation from some reference lattice spacing is separated out as the magnetoelastic energy.<sup>4</sup>

To reemphasize, the purpose of the previous physical discussion of the microscopic origins of the various energy terms was to guide in the selection of an adequate set of thermodynamic variables. The energy will then be a function of these variables. It was concluded that the gradient of the magnetization is a reasonable choice for the continuum dependence of the exchange energy. The anisotropy energy depended on the orientation of the elemental magnetic moment within the unit cell. Hence, the magnetization vector is the logical variable. For the elastic strain, the deformation gradients will be

selected. The functional dependence of the local energy density is

$$\epsilon_{\text{LOC}} \left( \frac{\partial x_i}{\partial a_j}, \alpha_i, \frac{\partial \alpha_i}{\partial a_j} \right), \quad (2.9)$$

where  $x_i$  are the space or Eulerian coordinates and  $a_j$  are the material or Lagrangian coordinates.<sup>27</sup> It should be noted that in a purely phenomenological formulation higher order derivatives of  $x_i$  and  $\alpha_i$  should properly be included.

#### 2.4. Phenomenological Expression

A phenomenological expansion of the energy in a Taylor series at this point would be premature. The problem is that  $\epsilon_{\text{LOC}}$  cannot be an arbitrary function of the chosen variables but must satisfy the physically obvious invariance of a rigid rotation of the mass element  $dm$ . This would restrict the form of the property tensors obtained from the Taylor expansion. To circumvent this problem, the functional dependence of  $\epsilon_{\text{LOC}}$  will be recast in terms of new variables under which  $\epsilon_{\text{LOC}}$  can be an arbitrary function.<sup>28</sup> This will be accomplished with a theorem due to Cauchy.<sup>29</sup>

Theorem--Any function,  $f(\vec{v}_1, \dots, \vec{v}_n)$ , invariant under a rigid rotation of the system of vectors,  $\vec{v}_1, \dots, \vec{v}_n$ , can be expressed as a function of the various quantities  $\vec{v}_\alpha \cdot \vec{v}_\beta$  ( $\alpha, \beta$  same or different) or  $\vec{v}_\alpha \cdot \vec{v}_\beta \times \vec{v}_\gamma$  ( $\alpha, \beta$ , and  $\gamma$  different).

$\epsilon_{\text{LOC}}$  is a function of seven vectors.

$$\epsilon_{\text{LOC}} = \epsilon_{\text{LOC}} \left( \frac{\partial \vec{r}}{\partial a_1}, \frac{\partial \vec{r}}{\partial a_2}, \frac{\partial \vec{r}}{\partial a_3}, \vec{\alpha}, \frac{\partial \vec{\alpha}}{\partial a_1}, \frac{\partial \vec{\alpha}}{\partial a_2}, \frac{\partial \vec{\alpha}}{\partial a_3} \right)$$

A sufficient choice of independent variables from Cauchy's theorem gives the functional dependence

$$\epsilon_{\text{LOC}}(E_{ij}, \alpha_i^*, G_{ij})$$

where

$$E_{ij} = \frac{1}{2} \left( \frac{\partial x_k}{\partial a_i} \frac{\partial x_k}{\partial a_j} - \delta_{ij} \right) \quad (2.10)$$

is the finite strain tensor,

$$\alpha_i^* = \frac{\partial x_k}{\partial a_i} \alpha_k, \quad (2.11)$$

and

$$G_{ij} = \frac{\partial \alpha_k}{\partial a_i} \frac{\partial \alpha_k}{\partial a_j}. \quad (2.12)$$

These thermodynamic variables are not the only ones allowed by Cauchy's theorem but are the ones usually selected. (See Brown<sup>5</sup> for a more fundamental set.)

In terms of these variables,  $\epsilon_{\text{LOC}}$  is arbitrary. A phenomenological expansion in the usual manner yields<sup>30</sup>

$$\begin{aligned} \epsilon_{\text{LOC}} &= \epsilon_{\text{LOC}}^0(S) + g(\alpha_p^*, S) + g_{ij}(\alpha_p^*, S)E_{ij} + \frac{1}{2!} g_{ijkl}(\alpha_p^*, S)E_{ij}E_{kl} \\ &\quad + \frac{1}{3!} g_{ijklmn}(\alpha_p^*, S)E_{ij}E_{kl}E_{mn} + \dots + \lambda_{ij}G_{ij} + \lambda_{ijkl}E_{ij}G_{kl} \\ &\quad + \dots \end{aligned}$$

where

$$g(\alpha_p^*, S) = K_{ij}\alpha_i^*\alpha_j^* + \frac{1}{2!} K_{ijkl}\alpha_i^*\alpha_j^*\alpha_k^*\alpha_l^* + \dots,$$

$$g_{ij}(\alpha_p^*, S) = \beta_{ij}(S) + b_{ijkl}\alpha_k^*\alpha_l^* + \frac{1}{2!} b_{ijklmn}\alpha_k^*\alpha_l^*\alpha_m^*\alpha_n^* + \dots,$$

$$g_{ijkl}(\alpha_p^*, S) = C_{ijkl} + B_{ijklmn}\alpha_m^*\alpha_n^* + \dots,$$

and

$$g_{ijklmn}(\alpha_p^*, S) = C_{ijklmn} + \dots.$$

The various phenomenological constants relate to physical properties and have been accordingly named. The following catalogues those material properties.

$K_{ij}$ , $K_{ijkl}$	-- various order anisotropy constants
$\beta_{ij}(S)$	-- related to thermal strains
$b_{ijkl}$	-- first order magnetostrictive constants
$b_{ijklmn}$	-- Becker-Doring constants
$C_{ijkl}$	-- adiabatic elastic moduli
$B_{ijklmn}$	-- second order ME constants
$C_{ijklmn}$	-- third order elastic moduli
$\lambda_{ij}$	-- exchange constants
$\lambda_{ijkl}$	-- exchange striction constants

The number of independent elements in the property tensors is reduced by invoking symmetry requirements. They are thermodynamic symmetry which equates certain derivatives of the energy by interchanging the order of differentiation, crystal symmetry which is determined by operators of the crystal class of interest, and magnetic symmetry which is determined by the particular magnetic point group. The expression for cubic symmetry<sup>30</sup> (which includes YIG), correct to second order in magnetoelastic terms and third order in mechanical terms, is

$$\begin{aligned}
\varepsilon_{\text{LOC}} = & \varepsilon_{\text{LOC}}^0(S) + \beta(E_{11} + E_{22} + E_{33}) + \frac{1}{2} C_{11}(E_{11}^2 + E_{22}^2 + E_{33}^2) \\
& + C_{12}(E_{11}E_{22} + E_{22}E_{33} + E_{33}E_{11}) + 2C_{44}(E_{23}^2 + E_{31}^2 + E_{12}^2) \\
& + \frac{1}{6} C_{111}(E_{11}^3 + E_{22}^3 + E_{33}^3) + \frac{1}{2} C_{112}(E_{11}^2(E_{22} + E_{33}) + E_{22}^2(E_{33} + E_{11})) \\
& + E_{33}^2(E_{11} + E_{22}) + C_{123}E_{11}E_{22}E_{33} + 2C_{144}(E_{11}E_{23}^2 + E_{22}E_{31}^2 + E_{33}E_{12}^2) \\
& + 2C_{155}((E_{11} + E_{22})E_{12}^2 + (E_{22} + E_{33})E_{23}^2 + (E_{33} + E_{11})E_{31}^2) \\
& + b_{11}(E_{11}^{*\alpha_1^2} + E_{22}^{*\alpha_2^2} + E_{33}^{*\alpha_3^2}) + 2b_{44}(E_{23}^{*\alpha_2^*\alpha_3^*} + E_{31}^{*\alpha_3^*\alpha_1^*} \\
& + E_{12}^{*\alpha_1^*\alpha_2^*}) + \frac{1}{2} B_{111}(E_{11}^{*\alpha_1^2} + E_{22}^{*\alpha_2^2} + E_{33}^{*\alpha_3^2}) + B_{123}(E_{11}E_{22}^{*\alpha_3^2} \\
& + E_{22}E_{33}^{*\alpha_1^2} + E_{33}E_{11}^{*\alpha_2^2}) + 2B_{144}(E_{11}E_{23}^{*\alpha_2^*\alpha_3^*} + E_{22}E_{31}^{*\alpha_3^*\alpha_1^*} \\
& + E_{33}E_{12}^{*\alpha_1^*\alpha_2^*}) + 2B_{155}((E_{11} + E_{22})E_{12}^{*\alpha_1^*\alpha_2^*} + (E_{22} + E_{33})E_{23}^{*\alpha_2^*\alpha_3^*} \\
& + (E_{33} + E_{11})E_{31}^{*\alpha_3^*\alpha_1^*}) + 2B_{441}(E_{23}^{*\alpha_1^2} + E_{31}^{*\alpha_2^2} + E_{12}^{*\alpha_3^2}) \\
& + 4B_{456}(E_{23}E_{31}^{*\alpha_1^*\alpha_2^*} + E_{31}E_{12}^{*\alpha_3^*\alpha_2^*} + E_{12}E_{23}^{*\alpha_1^*\alpha_3^*}) + K_1(\alpha_1^{*\alpha_2^2} + \\
& + \alpha_2^{*\alpha_3^2} + \alpha_3^{*\alpha_1^2}) + \frac{2\pi\lambda}{M_s^2} \left( |\vec{\nabla}_a \alpha_1|^2 + |\vec{\nabla}_a \alpha_2|^2 + |\vec{\nabla}_a \alpha_3|^2 \right) \quad (2.13)
\end{aligned}$$

Keeping terms to lowest order, although not entirely consistently, one obtains the original expression of Becker and Doring<sup>3</sup> from conventional magnetoelastic theory plus the exchange energy.

$$\begin{aligned}
 \epsilon_{\text{LOC}} = & \frac{1}{2} c_{11}(e_{11}^2 + e_{22}^2 + e_{33}^2) + c_{12}(e_{11}e_{22} + e_{22}e_{33} + e_{33}e_{11}) \\
 & + 2c_{44}(e_{23}^2 + e_{31}^2 + e_{12}^2) + b_1(e_{11}\alpha_1^2 + e_{22}\alpha_2^2 + e_{33}\alpha_3^2) \\
 & + 2b_2(e_{12}\alpha_1\alpha_2 + e_{23}\alpha_2\alpha_3 + e_{31}\alpha_3\alpha_1) + K_1(\alpha_1^2\alpha_2^2 + \alpha_2^2\alpha_3^2 \\
 & + \alpha_3^2\alpha_1^2) + A\left(\left|\vec{\nabla}\alpha_1\right|^2 + \left|\vec{\nabla}\alpha_2\right|^2 + \left|\vec{\nabla}\alpha_3\right|^2\right)
 \end{aligned} \tag{2.14}$$

where  $b_1 = b_{11}$ ,  $b_2 = b_{44}$ , and  $A = 2\pi\lambda/M_s^2$ .

There is a reason for developing the energy expression through a finite strain formalism. The conventional magnetoelastic energy expression, Equation (2.14), was obtained by adding the energy of a magnetic rigid solid to the energy of a nonmagnetic elastic solid and then superposing an interaction term to describe the magnetoelastic effect. It has been pointed out that this expression does not contain sufficient terms to properly account for the energy to the order of strain assumed.<sup>5</sup> The success of the conventional magnetoelastic expression can be attributed to the extremely low strains ( $\sim 10^{-5}$ ) existing in usual magnetostrictive phenomenon. One worries whether it will be sufficient to describe the behavior for the quite high strains ( $\sim 10^{-2}$ ) which prevail in the present inverse magnetostrictive effect. Although conventional magnetoelastic theory will be used in the subsequent chapter, the effect of finite strain will be seriously considered in the appendix.

In summary, a complete energy expression for an anisotropic ferromagnet has been obtained.

$$E = \int (\epsilon_{\text{LOC}} - \frac{1}{2} \vec{H}_d \cdot \vec{M} - \vec{H}_e \cdot \vec{M}) dV \tag{2.15}$$

With this expression and thermodynamic equilibrium and stability criteria, magnetic equilibrium properties can, in principle, be predicted.

## CHAPTER III

### APPLICATION TO THE SHOCK INDUCED ANISOTROPY EFFECT

Passage of a shock wave through an infinite half space of ferromagnetic material creates, behind the shock, an infinite slab of ferromagnetic material in a state of uniaxial magnetic anisotropy normal to the plane of the slab. An external magnetic field is applied along a direction in the plane of the slab and, hence, orthogonal to the axis of uniaxial strain as seen in Figure 3.1. This chapter will utilize the thermodynamic tools developed in the preceding chapter to predict the magnetic behavior of a ferromagnet subject to this unique effect.

To proceed from the given energy expression to the final prediction of a magnetization curve in a given magnetic problem requires considerable effort and has been the subject of much theoretical investigation for many years. There have been basically two theoretical approaches to the problem. The more

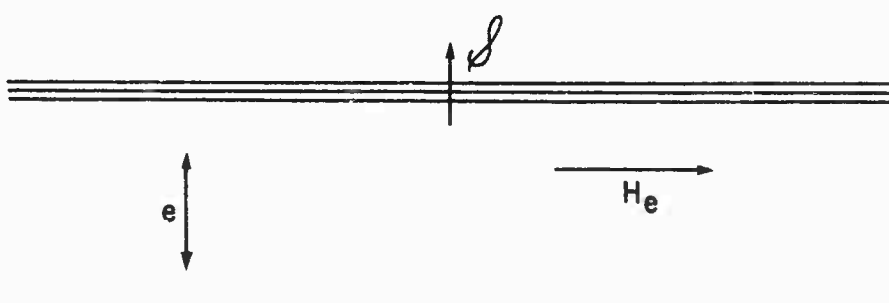


Fig. 3.1.--Shock created anisotropic ferromagnet.

contemporary theory is referred to as micromagnetism.<sup>31</sup> It assaults the energy minimization problem through calculus of variation techniques. This theory is more general; capable, in principle, of predicting domain walls, hysteresis, Barkhausen jumps, and other characteristic ferromagnetic properties. Its usefulness, however, is limited by the extreme complexity of the mathematics involved and little progress has been made except in the simplest geometries.

The other approach is domain theory.<sup>4,32</sup> It has enjoyed wider acceptance due to its ability to provide useful predictions in practical magnetic problems. Domain theory avoids the difficult mathematics brought about by the calculus of variation methods. This is accomplished by postulating the presence of domain walls in the material and considering the exchange energy as localized in these walls. Success of this theory rests on the ingenuity and experience of the theoretician since he must determine by extratheoretical consideration the domain geometry which will create the lowest energy.

This chapter will proceed by considering the shock induced anisotropy effect in single crystal material. The problem will be analyzed with established tools of domain theory and by these methods will be carried to its logical conclusion. The next step toward predicting the magnetic behavior in real material is the consideration of a theoretically dense polycrystal with random texture. This problem is explored and the averaging procedures relating single crystal behavior to polycrystal behavior are defined. Following this will be a brief review of the success of micromagnetic theory in exploring the anisotropy effect. In the last section the perturbing problem of porosity, present in all natural material, is considered.

### 3.1. Domain Theoretical Calculation (Single Crystal)

Consistent with domain theory, the volume integral in the energy expression for the anisotropic ferromagnet will be ignored. Instead, the total energy sufficient for predicting magnetic equilibrium states will be written.

$$\epsilon = \epsilon_{ex} + \epsilon_A + \epsilon_d + \epsilon_H$$

where each term refers to an energy density. The first term is the exchange energy while the second is the crystalline and magnetoelastic anisotropy energy.  $\epsilon_d = -\frac{1}{2} \vec{H}_d \cdot \vec{M}$  is the demagnetizing energy.  $\epsilon_H = -\vec{H}_e \cdot \vec{M}$  is the additional term included by the Legendre transformation and is just the interaction energy of the ferromagnet with the external magnetic field. It will be necessary to obtain each term for the problem of interest.

The total anisotropy energy from conventional magnetoelastic theory is

$$\begin{aligned} \epsilon_A = & K_1(\alpha_1^2 \alpha_2^2 + \alpha_2^2 \alpha_3^2 + \alpha_3^2 \alpha_1^2) + b_1(\alpha_1^2 e_{11} + \alpha_2^2 e_{22} + \alpha_3^2 e_{33}) \\ & + 2b_2(\alpha_1 \alpha_2 e_{12} + \alpha_2 \alpha_3 e_{23} + \alpha_3 \alpha_1 e_{31}). \end{aligned}$$

Uniaxial strain along a line colinear with the unit vector  $\vec{n}$  can be written in the tensor form

$$e_{ij} = e n_i n_j$$

where  $e = (\rho_0/\rho) - 1$  is the extension<sup>27</sup> along the direction of uniaxial strain.  $\vec{n}$  is arbitrarily oriented with respect to the crystal axis. In the present work, interest lies in shock induced anisotropy. In shock wave studies, strains in the large elastic and plastic regions are obtained. Thus, for many magnetic materials, the crystalline anisotropy energy is 10 to 30 times smaller than the induced anisotropy energy in this strain region.

Therefore, the crystalline anisotropy energy will be ignored. The anisotropy energy of interest becomes

$$\begin{aligned}\epsilon_{me} = & b_1 e(\alpha_1^2 n_1^2 + \alpha_2^2 n_2^2 + \alpha_3^2 n_3^2) + 2b_2 e(\alpha_1 \alpha_2 n_1 n_2 \\ & + \alpha_2 \alpha_3 n_2 n_3 + \alpha_3 \alpha_1 n_3 n_1).\end{aligned}\quad (3.1)$$

To proceed with the domain theory analysis of the shock induced anisotropy effect, two single crystal problems will be treated concurrently. These will be called the  $\langle 100 \rangle$  problem and the  $\langle 111 \rangle$  problem. The  $\langle 100 \rangle$  problem corresponds to a state of uniaxial strain along a  $\langle 100 \rangle$  axis with a perpendicular applied field. The  $\langle 111 \rangle$  problem corresponds to a state of uniaxial strain along a  $\langle 111 \rangle$  axis with a perpendicular applied field. These two fundamental problems have their analogs in the thermodynamic inverse of this effect. They are magnetostriction along the  $\langle 100 \rangle$  and  $\langle 111 \rangle$  axes.<sup>4</sup> The magnetoelastic constants,  $b_1$  and  $b_2$ , will be found to relate in a similar way to the magnetostriction constants,  $\lambda_{100}$  and  $\lambda_{111}$ .

In the spirit of domain theory, models for the domain structure must be postulated. Energies corresponding to each model are then obtained and compared. From this, conclusions are drawn as to the most probable domain structure. Figure 3.2 shows the domain structure models which will be considered. Domain walls normal to the strain axis are not expected. This is because the variation in the magnetization direction through the domain wall cannot be made without allowing  $\vec{\nabla} \cdot \vec{M}$  to deviate from zero.  $\vec{\nabla} \cdot \vec{M} \neq 0$  in the domain wall implies magnetic volume poles in the wall and, hence, a high demagnetizing energy. This would be energetically unfavorable. Domains of closure are not expected due to the high induced anisotropy energy.

### 3.1.1. Induced Anisotropy Energy

The induced anisotropy energies for the  $\langle 100 \rangle$  problem and the  $\langle 111 \rangle$  problem will be obtained in this section. The energy will be obtained within domains and within the walls through which the transition between adjacent domains is made. This will be done for walls of the form shown in Figure 3.2(a) and Figure 3.2(b).

Consider first the  $\langle 100 \rangle$  problem and the domain walls in Figure 3.2(a). Transform Equation (3.1) to polar coordinates using

$$\alpha_1 = \sin\theta\cos\phi, \quad \alpha_2 = \sin\theta\sin\phi, \quad \text{and} \quad \alpha_3 = \cos\theta.$$

The induced anisotropy energy in a domain is easily obtained.

$$\epsilon_{me}^{\langle 100 \rangle}(\text{domain}) = b_1 e \sin^2\theta.$$

To obtain the induced anisotropy energy in the wall, the variation in  $\vec{M}$  through the wall must be considered. The requirement that  $\vec{\nabla} \cdot \vec{M} = 0$  through the wall is equivalent to demanding that  $\theta$  be constant through the wall. The transition between adjacent domains then proceeds by a rotation of  $\phi$  from 0 to  $\pi$ . The energy in the wall is

$$\epsilon_{me}^{\langle 100 \rangle} = b_1 e \sin^2\theta \cos^2\phi.$$

A slightly more difficult analysis gives for the  $\langle 111 \rangle$  problem

$$\epsilon_{me}^{\langle 111 \rangle}(\text{domain}) = b_2 e \sin^2\theta$$

and

$$\epsilon_{me}^{\langle 111 \rangle} = b_2 e \sin^2\theta \cos^2\phi.$$

Since the form of the energies is the same for the  $\langle 100 \rangle$  problem and the  $\langle 111 \rangle$  problem, we will write

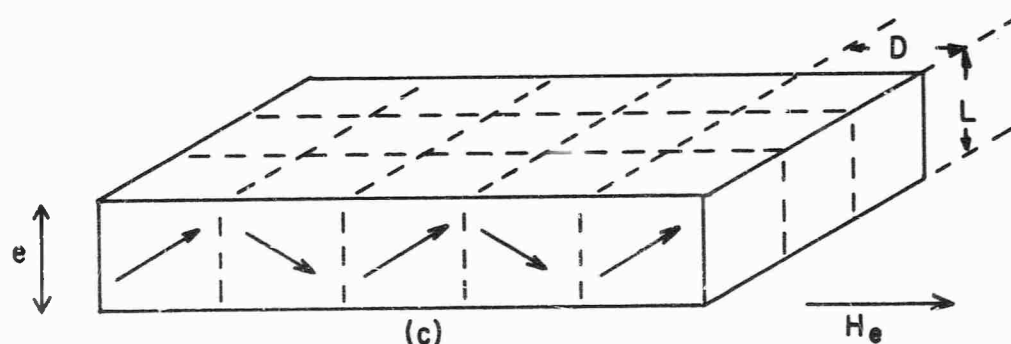
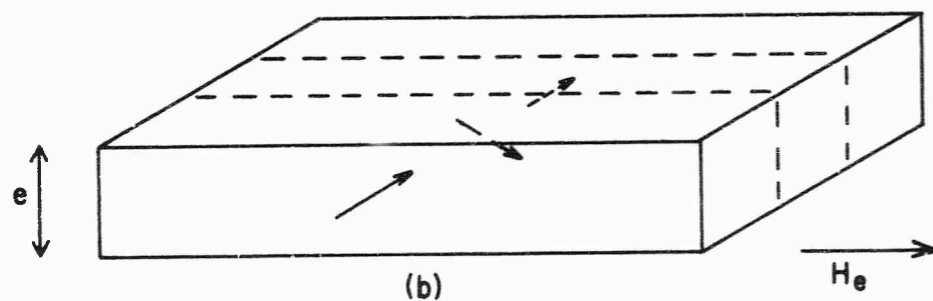
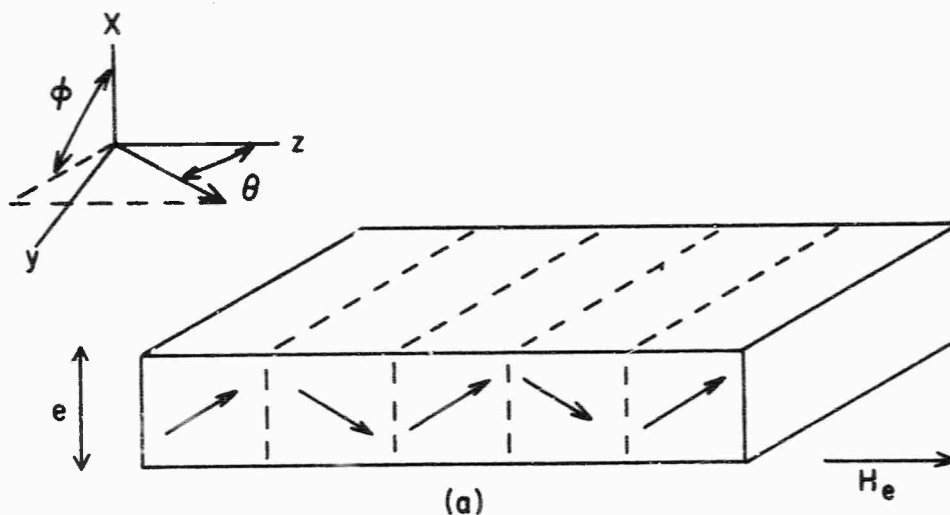


Fig. 3.2.--(a) Model for plate-like domain structure perpendicular to the applied field  
 (b) Model for plate-like domain structure parallel to the applied field  
 (c) Model for needle shaped domain structure oriented along axis of uniaxial strain. Polar angles define direction of magnetization during transition through domain wall.

$$\epsilon_{me}(\text{domain}) = b \epsilon \sin^2 \theta \quad (3.2)$$

and

$$\epsilon_{me} = b \epsilon \sin^2 \theta \cos^2 \phi \quad (3.3)$$

where  $b = b_1$  or  $b_2$  for the  $\langle 100 \rangle$  problem or the  $\langle 111 \rangle$  problem, respectively.

Consider the domain configuration in Figure 3.2(b). Again the energy in the domain is

$$\epsilon_{me}(\text{domain}) = b \epsilon \sin^2 \theta.$$

The transition through the wall proceeds in the  $(x, z)$  plane by varying  $\xi$  continuously from  $-\theta$  to  $\theta$ . The energy in the wall is

$$\epsilon_{me} = b \epsilon \sin^2 \xi, \quad -\theta \leq \xi \leq \theta. \quad (3.4)$$

Equation (3.2), Equation (3.3), and Equation (3.4) are the primary equations derived in this section.

### 3.1.2. Exchange Energy

Within the concepts of domain theory, the exchange energy is believed to reside only in the domain walls or transition regions between adjacent domains. The usual method for obtaining this domain wall energy is through a Landau-Lifshitz domain wall calculation.<sup>33</sup> This has been fully developed in the literature<sup>22,32</sup> and will be described only briefly here. The method consists of writing a one dimensional integral expression for the energy in the transition region between domains. The terms which contribute to the wall energy are the exchange energy and the excess crystalline or magnetoelastic anisotropy energy incurred by the transition through the wall. It is assumed

that  $\vec{\nabla} \cdot \vec{M} = 0$  ( $\theta = \text{constant}$ ) holds through the wall. This one dimensional integral energy expression is minimized by variational calculus. The result predicts that at all points within the wall the exchange energy is equal to the excess anisotropy energy. It is found that the wall energy per unit area is given by

$$\sigma_w = 2\sqrt{A} \sin\theta \int_{\phi_1}^{\phi_2} |(\epsilon_{me}(\text{domain}) - \epsilon_{me})^{1/2}| d\phi. \quad (3.5)$$

The crystal anisotropy energy has not been considered.  $A$  is again the exchange constant and  $\phi_1$  and  $\phi_2$  are the azimuthal orientation of the magnetization in the adjacent domains separated by the wall.

In this section, the domain wall energies in Figure 3.2(a) and Figure 3.2(b) will be obtained. They will be called  $\sigma_w^S$  and  $\sigma_w^P$ , respectively. For Figure 3.2(a), using Equation (3.2) and Equation (3.3) with Equation (3.5) gives

$$\sigma_w^S = 2\sqrt{A|\beta\epsilon|} \sin^2\theta \int_0^{\pi} \sin\phi d\phi$$

or

$$\sigma_w^S = 4\sqrt{A|\beta\epsilon|} \sin^2\theta \quad (3.6)$$

For Figure 3.2(b), using Equation (3.2) and Equation (3.4) with Equation (3.5) gives

$$\sigma_w^P = 2\sqrt{A|\beta\epsilon|} \int_{-\theta}^{\theta} (\sin^2\theta - \sin^2\xi)^{1/2} d\xi.$$

Making the substitution

$$\sin x = \sin\theta \sin\xi = a \sin\xi$$

and using the identity

$$\cos^2 x = \left(1 - \frac{1}{a^2}\right) + \frac{1}{a^2} (1 - a^2 \sin^2 x),$$

one obtains

$$\sigma_w^p = 4\sqrt{A|\beta e|}(a^2 - 1) \int_0^{\pi/2} \frac{dx}{(1 - a^2 \sin^2 x)^{1/2}} + \int_0^{\pi/2} (1 - a^2 \sin^2 x)^{1/2} dx.$$

This is

$$\sigma_w^p = 4\sqrt{A|\beta e|}((a^2 - 1) K(a, \pi/2) + E(a, \pi/2))$$

where  $a = \sin\theta$  and  $K$  and  $E$  are complete elliptic integrals of the first and second kind.

$\sigma_w^s$  and  $\sigma_w^p$  are compared in Figure 3.3. It is seen that the domain model considered in Figure 3.2(b) yields a slightly lower energy. In actual crystalline material, imperfections such as dislocation, impurity, etc. can significantly alter the domain wall energy. For this reason, it is believed that the slight energy difference does not justify the prediction of the domain structure in Figure 3.2(b) over that in Figure 3.2(a). From this, one may conclude that domain theory suggests a needle or sliver shaped domain structure oriented along the axis of uniaxial strain will nucleate behind the shock front. A model for this structure is shown in Figure 3.2(c).

Due to the much simpler form of Equation (3.6), the approximation

$$\sigma_w^p \approx \sigma_w^s = \sigma_w = 4\sqrt{A|\beta e|} \sin^2 \theta$$

will be made. An expression for the effective exchange energy density is given by

$$\epsilon_{ex} = \frac{2\sigma_w}{D}$$

or

$$\epsilon_{ex} = \frac{8\sqrt{A|be|}}{D} \sin^2 \theta$$

where  $D$  is the dimension of a domain as shown in Figure 3.2(c).

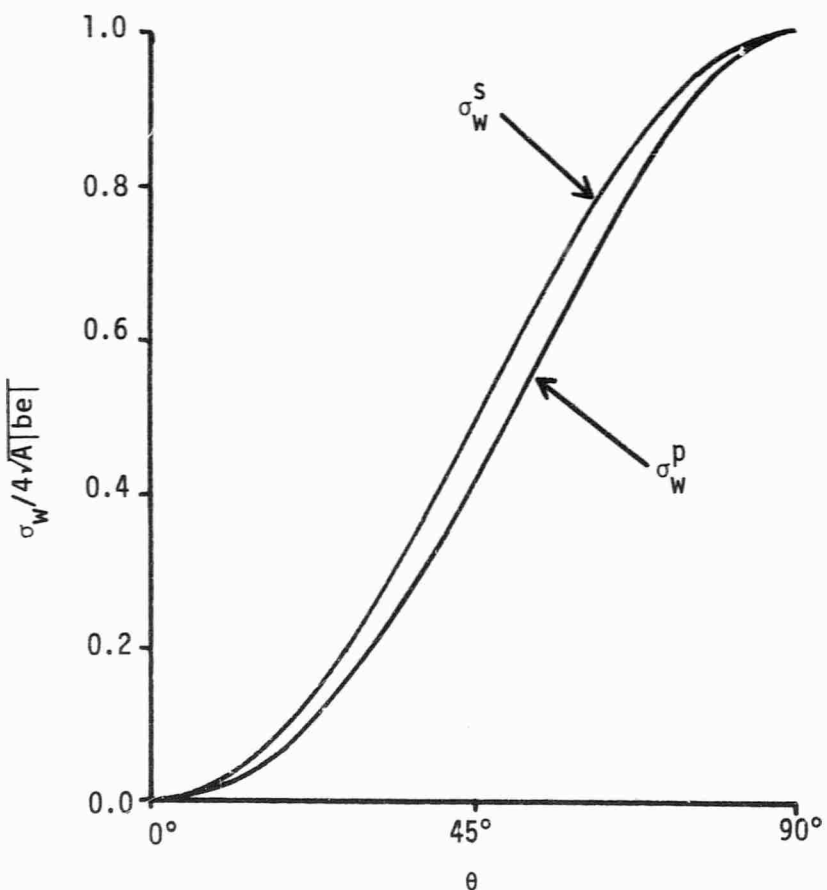


Fig. 3.3.--Domain wall energy as a function of  $\theta$ .  
 $\sigma_w^s$  corresponds to the wall geometry in Fig. 3.2(a);  $\sigma_w^p$  corresponds to the wall geometry in Fig. 3.2(b).

### 3.1.3. Demagnetizing Energy

The demagnetizing energy can be obtained by solving the magnetostatic boundary value problem for the magnetic surface pole distribution on two surfaces separated a distance  $L$  as is indicated in Figure 3.2(c). The solution requires only a slight variation on a problem already solved by Kittel.<sup>4</sup> Only the result will be reported here. It is approximately given by

$$\mathcal{E}_d = 1.1 \frac{DM_s^2}{L} \sin^2 \theta.$$

The approximation results from terminating an infinite series. Again  $L$  is the slab thickness,  $D$  is the domain dimension, and  $M_s$  is the saturation magnetization.

### 3.1.4. Total Energy

From the results of Sections 3.1.1, 3.1.2, and 3.1.3, the total thermodynamic energy for the ferromagnetic material behind the shock front can be explicitly written. The total energy is

$$\mathcal{E}(D, \theta) = -M_s H_e \cos \theta + b e \sin^2 \theta + 1.1 \frac{DM_s^2}{L} \sin^2 \theta + \frac{8\sqrt{A}be}{D} \sin^2 \theta. \quad (3.7)$$

Equilibrium thermodynamics predicts that the energy expression,  $\mathcal{E}(D, \theta)$ , will be a minimum with respect to a variation of the internal coordinates,  $D$  and  $\theta$ . Consider the domain width parameter first. Minimizing with respect to  $D$  gives

$$\frac{\partial \mathcal{E}}{\partial D} = 1.1 \frac{M_s^2}{L} \sin^2 \theta - \frac{8\sqrt{A}be}{D^2} \sin^2 \theta = 0.$$

This yields an expression for the domain width.

$$D = \left( \frac{8L\sqrt{A|be|}}{1.1 M_s^2} \right)^{1/2}$$

This can be substituted into Equation (3.7) giving

$$\epsilon(\theta) = -M_s H_e \cos\theta + be \sin^2\theta + 2 \left( \frac{8.8 M_s^2 \sqrt{A|be|}}{L} \right)^{1/2} \sin^2\theta$$

or

$$\epsilon(\theta) = -M_s H_e \cos\theta + be \sin^2\theta + \gamma |e|^{1/4} \sin^2\theta \quad (3.8)$$

where

$$\gamma = 2 \left[ \frac{8.8 M_s^2 \sqrt{A|b|}}{L} \right]^{1/2}.$$

The last term in Equation (3.8) will be called the equilibrium exchange and demagnetizing energy.

At this point a discussion of the results obtained so far is warranted. An estimate of the exchange constant can be obtained from molecular field theory.<sup>22</sup> This is

$$A \approx \frac{3kT_c}{za}$$

where  $k$  is Boltzmann's constant,  $T_c$  is the Curie or Néel temperature,  $z$  is the number of nearest neighbors, and  $a$  is the lattice constant. This gives  $A = 3 \times 10^{-7}$  erg/cm in YIG. At a strain of  $-0.01$  in YIG which corresponds to a shock pressure of about 25 kilobars, the predicted domain width is approximately 20  $\mu$ ron. This is in agreement with other work.<sup>11</sup> The equilibrium exchange and demagnetizing energy in Equation (3.8) is observed to increase as the fourth root of the strain while the induced anisotropy

energy increases linearly with the strain. This suggests that the equilibrium exchange and demagnetizing energy is about 2% of the induced anisotropy energy. This justifies ignoring the equilibrium exchange and demagnetizing energy in predicting magnetic behavior in the region of large elastic and plastic strain in YIG as was done by Royce<sup>7</sup> and Bartel.<sup>10</sup> It is realized that this statement need not hold true for all materials.

From the total thermodynamic energy, Equation (3.8), the equilibrium magnetization curve can be obtained. Thermodynamic equilibrium demands that

$$\frac{d\mathcal{E}}{d\theta} = 0.$$

This has two solutions;

$$\sin\theta = 0$$

and, ignoring exchange and dipolar energy,

$$2be \cos\theta + H_e M_s = 0.$$

Thermodynamic stability requires that

$$\frac{d^2\mathcal{E}}{d\theta^2} = 2be(\cos^2\theta - \sin^2\theta) + H_e M_s \cos\theta > 0$$

at the equilibrium solution. For the solution  $\sin\theta = 0$ , this implies that

$$2be + H_e M_s > 0.$$

Under shock induced anisotropy, this would always be the stable solution for material with negative magnetoelastic constants. For material with positive magnetoelastic constants, this solution becomes unstable at a nucleation field of  $H_{nuc} = -2be/M_s$ . The subsequent behavior is then given by the

second equilibrium solution. The predicted magnetization curve is

$$\frac{M}{M_s} = \begin{cases} 1 & \text{for } H_e > -\frac{2be}{M_s} \\ -\frac{M_s}{2be} H_e & \text{for } H_e < -\frac{2be}{M_s} \end{cases} \quad (3.9)$$

where  $M/M_s = \cos\theta$  and  $b = b_1$  for the  $\langle 100 \rangle$  problem or  $b = b_2$  for the  $\langle 111 \rangle$  problem. The curves are shown in Figure 3.5.

### 3.2. Domain Theoretical Calculation (Polycrystal)

This development will proceed by considering the equivalent shock induced anisotropy effect in theoretically dense isotropic cubic polycrystalline ferromagnetic material. This will be accomplished from knowledge of the single crystal magnetic properties. Also, this should be a better approximation than the single crystal analysis of the preceding section to the magnetic behavior of commercial and natural material subject to this effect.

The prediction of a polycrystalline material property from its equivalent single crystal property is a problem confronted in many areas of physics. The approach, quite similar in every case, requires an averaging of the single crystal property for an arbitrarily oriented crystallite over all crystal orientations.<sup>34</sup> The complicating factor is that an arbitrary crystallite interacts, not only with the external forces, but also with other grains in the polycrystal. This grain-grain interaction can be mechanical (through stresses), electrical, or magnetic. In most cases, this complicated interaction is not known.

Examples are elastic constants, dielectric constants, magnetostriction constants, and conductivities. In each case basic assumptions concerning the grain-grain interaction must be defined before progress can be made. For

instance, in the case of elastic constants,<sup>35</sup> two assumptions have been used. One assumption is that uniform strain<sup>36</sup> exists throughout the crystal. The other is that uniform stress<sup>37</sup> prevails. Experiment favors neither, usually being closer to an arithmetic average of the results of the two assumptions. The same assumptions are made in obtaining polycrystalline magnetostriction constants.<sup>38,39,40,41</sup> In this case experiment favors the assumption of uniform stress.

In the present problem, the state of strain behind a plane shock wave in a theoretically dense cubic polycrystal is assumed to be uniform. (See Appendix V.) The speculation involves the magnetic grain-grain interaction. This is a complicated many body interaction of current interest<sup>42,43</sup> about which little is known. In analogy to the previous examples, this development will define the extreme assumptions regarding the grain-grain interaction and then consider each individually.

One extreme is that material crystallites interact with sufficient strength to cause a cooperative, colinear alignment of the grains' magnetization vectors. The other extreme is that grain-grain interactions are negligible and that each grain individually seeks equilibrium determined by the requirements of the anisotropy field and external magnetic field. These assumptions will be called the interacting grain assumption and the independent grain assumption, respectively.

### 3.2.1. Interacting Grain Assumption

The interacting grain assumption will be considered first. This assumption was made by Royce<sup>7,8</sup> during pioneering work on the shock induced anisotropy effect and leads to a mathematically tractable averaging process.

Domain structure in a polycrystalline ferromagnet is usually on an intra-grain scale.<sup>44</sup> This is due to high crystal anisotropy energy and large

angle grain boundaries which make continuous domains across grain boundaries energetically unfavorable. There are cases, however, such as in material subject to cold working, in which a high degree of crystal orientation allows an extra-grain domain structure.<sup>4</sup> In the present effect, the easy direction of magnetization is determined not only by the crystallographic axis but also by the direction of uniaxial strain. Thus, the effect of the shock wave is to create a condition of magnetic texture defined by the direction of uniaxial strain behind the shock wave. It would not be implausible to expect an extra-grain domain structure to nucleate after passage of the shock wave.

A further argument for this assumption follows by considering a spherical grain interior to a domain of uniform magnetization. The magnetization in this grain could deviate from this direction of uniform magnetization only by creating surface poles on the grain boundary. The energy associated with this is

$$\epsilon = - \frac{4\pi}{3} M_s^2 \cos\theta.$$

In YIG, at typical shock stresses, this energy is of the same order as the strain induced anisotropy energy. Hence, there will be strong torques attempting to maintain uniform magnetization throughout the domain.

The following assumption simplifies the averaging process and creates a neat form for the magnetoelastic energy of a polycrystal. It is assumed that  $\overset{\rightarrow}{M} \cdot \overset{\rightarrow}{n}_e$  is uniform throughout the field.

To proceed with the averaging process, the six dependent variables,  $\alpha_1$ ,  $\alpha_2$ ,  $\alpha_3$ ,  $n_1$ ,  $n_2$ , and  $n_3$ , appearing in the energy expression will be expressed in terms of four independent angular variables as shown in Figure 3.4.<sup>34,45</sup> The direction cosines are related to the angular variables by

$$\alpha_1 = \sin\lambda\cos\beta, \quad \alpha_2 = \sin\lambda\sin\beta, \quad \alpha_3 = \cos\lambda,$$

$$n_1 = \cos\xi\sin\lambda\cos\beta + \sin\xi(\cos\lambda\cos\beta\cos\psi + \sin\beta\sin\psi),$$

$$n_2 = \cos\xi\sin\lambda\sin\beta + \sin\xi(\cos\lambda\sin\beta\cos\psi - \cos\beta\sin\psi),$$

and

$$n_3 = \cos\xi\cos\lambda - \sin\xi\sin\lambda\cos\psi.$$

Since the polycrystal is isotropic,

$$\frac{1}{8\pi^2} \sin\lambda d\lambda d\beta d\psi$$

is the probability that the magnetization lies in the range  $\lambda$  to  $\lambda + d\lambda$  and  $\beta$  to  $\beta + d\beta$  while the strain is in a range  $\psi$  to  $\psi + d\psi$ . The average values of various terms appearing in the energy expression are obtained from

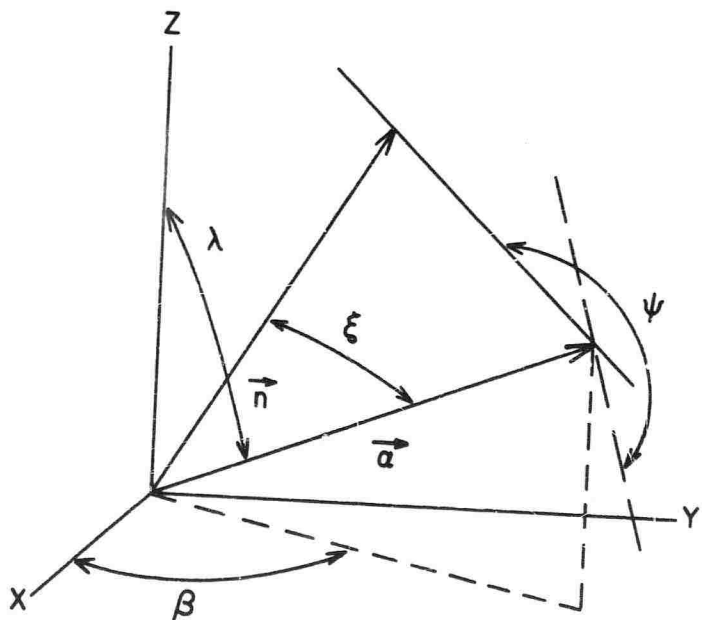


Fig. 3.4.--Independent angular coordinates for representing anisotropy energy.

$$\bar{f}(\xi) = \frac{1}{8\pi^2} \int_0^\pi \int_0^{2\pi} \int_0^{2\pi} f(\xi, \lambda, \beta, \psi) \sin \lambda d\lambda d\beta d\psi.$$

Various averages will be required and are tabulated in Table 1.

TABLE 1 --Average values of various terms appearing in the energy expression

$f(\xi, \lambda, \beta, \psi)$	$\bar{f}(\xi)$
$\alpha_1^2 \alpha_2^2 + \alpha_2^2 \alpha_3^2 + \alpha_3^2 \alpha_1^2$	$\frac{1}{5}$
$\alpha_1^2 n_1^2 + \alpha_2^2 n_2^2 + \alpha_3^2 n_3^2$	$\frac{1}{5} + \frac{2}{5} \cos^2 \xi$
$\alpha_1 \alpha_2 n_1 n_2 + \alpha_2 \alpha_3 n_2 n_3 + \alpha_3 \alpha_1 n_3 n_1$	$-\frac{1}{10} + \frac{3}{10} \cos^2 \xi$
$\alpha_1^2 n_1^4 + \alpha_2^2 n_2^4 + \alpha_3^2 n_3^4$	$\frac{3}{35} + \frac{12}{35} \cos^2 \xi$
$\alpha_1 \alpha_2 n_1 n_2 n_3^2 + \alpha_2 \alpha_3 n_2 n_3 n_1^2 + \alpha_3 \alpha_1 n_3 n_1 n_2^2$	$-\frac{1}{70} + \frac{3}{70} \cos^2 \xi$
$\alpha_1^2 \alpha_2^2 n_3^2 + \alpha_2^2 \alpha_3^2 n_1^2 + \alpha_3^2 \alpha_1^2 n_2^2$	$\frac{3}{35} - \frac{2}{35} \cos^2 \xi$

From this table, the average value of the anisotropy energy from conventional magnetoelastic theory, Equation (3.1), can immediately be written down. It is

$$\epsilon_A = \frac{1}{5} K_1 + B \cos^2 \xi. \quad (3.10)$$

where

$$B = \frac{2}{5} b_1 + \frac{3}{5} b_2.$$

The crystal anisotropy energy averages to a constant and does not contribute

to the effect. The total energy expression for a ferromagnetic polycrystal, assuming interacting grains, takes the simple form

$$\epsilon = B_e \sin^2 \theta - H_e M_s \cos \theta, \quad (3.11)$$

as in the single crystal cases with  $b$  replaced by  $B$ , since  $\theta$  and  $\xi$  are complementary angles. Thus, thermodynamic equilibrium predicts a linear equilibrium magnetization curve for the interacting grain assumption,

$$\frac{M}{M_s} = \begin{cases} 1, & H_e > -\frac{2B_e}{M_s} \\ -\frac{M_s}{2B_e} H_e, & H_e < -\frac{2B_e}{M_s} \end{cases} \quad (3.12)$$

intermediate between the extremes defined by the  $\langle 100 \rangle$  problem and the  $\langle 111 \rangle$  problem in the equivalent single crystal behavior.

### 3.2.2. Independent Grain Assumption

It is quite possible that the uniform magnetization field demanded by the previous assumption does not occur. The isolated single particle critical size within which a single domain exists for YIG is less than 1 micron. This size will increase for a bounded crystallite due to a substantial decrease in surface poles at the grain boundary, but not by more than an order of magnitude.<sup>42</sup> Also, the single crystal domain width predicted previously, Equation (3.8), was approximately 20 microns. The grain size of the material used in the present work ranged from 5 to 25 microns. This suggests that perhaps an intra-grain domain structure would nucleate in order to reduce magnetic poles which would otherwise collect heavily along grain boundaries.<sup>42,44</sup> This is usually the case for unstrained material and may possibly occur in the material behind the shock front. If an intra-grain domain structure occurred,

there would not be a prevailing magnetic field as was considered in the interacting grain assumption. In this case it would be more likely that each grain would distribute about some average depending on the orientation of its crystallographic axis with the external fields.

A simple consideration will show that, if independent grain conditions obtain, then the average magnetoelastic energy previously obtained in the interacting grain assumption is too high. The energy from the interacting grain assumption contained not only a part necessary to bring individual magnetic grains to their independent equilibrium positions, but also a part required to bring these magnetic grains into colinear alignment. Too large an induced anisotropy energy would then predict too much demagnetization.

The independent grain assumption is that each crystallite seeks equilibrium subject only to the requirements of the induced anisotropy field and the external magnetic field and independent of the behavior of neighboring crystallites. A rigorous approach to the averaging procedure would be to express the magnetization direction in the anisotropy energy expression, Equation (3.1), in terms of polar coordinates  $\theta$  and  $\phi$ . The total energy expression should then be minimized with respect to  $\theta$  and  $\phi$  for an arbitrarily oriented crystallite. The resulting magnetization projection along the direction of the applied field should then be averaged over all crystal orientations. This problem, which has been encountered previously in another context, cannot be solved explicitly for  $\theta$  and  $\phi$  and has not been completed.<sup>40</sup>

An alternate approach, in the spirit of calculations made by Lee,<sup>46</sup> is to write the average normalized magnetization,

$$\overline{\cos\theta} = \frac{\int F(\Omega) \cos\theta d\Omega}{\int F(\Omega) d\Omega}, \quad (3.13)$$

in terms of an unknown distribution function of the magnetization vector directions throughout the solid angle. A first harmonic assumption for the distribution function is that  $F(\Omega)$  is uniform throughout the solid angle defined by the extreme angles from the  $\langle 100 \rangle$  problem and the  $\langle 111 \rangle$  problem. These were

$$\cos\theta_1 = -\frac{M_s}{2b_1 e} H_e \quad \text{and} \quad \cos\theta_2 = -\frac{M_s}{2b_2 e} H_e.$$

$F(\Omega)$  is zero otherwise. This first harmonic approximation gives for the average value

$$\overline{\cos\theta} = \frac{\int_{\theta_1}^{\theta_2} \cos\theta \sin\theta d\theta}{\int_{\theta_1}^{\theta_2} \sin\theta d\theta} = \frac{\int_{x_1}^{x_2} x dx}{\int_{x_1}^{x_2} dx}$$

where  $x = \cos\theta$ . A problem occurs when  $\cos\theta_1$  is unity at which point the first grains reach saturation. To freeze the upper limit of integration artificially constrains the distribution function. This problem can be circumvented by allowing the upper limit to continue but demanding that the respective contribution to  $\cos\theta$  be unity. This gives

$$\overline{\cos\theta} = \begin{cases} \frac{x_1}{x_1 - x_2} & \text{for } x_1 \leq 1 \\ \frac{x_2}{x_1 - x_2} & \text{for } x_1 \geq 1. \end{cases}$$

x<sub>1</sub>  
 x dx  
 —————  
 x<sub>1</sub>  
 dx  
 x<sub>2</sub>  
 x<sub>1</sub>  
 x dx + —————  
 1  
 x<sub>2</sub>  
 x<sub>1</sub>  
 dx  
 x<sub>2</sub>

Performing the integration gives

$$\overline{\cos\theta} = \begin{cases} \frac{1}{2}(x_1 + x_2) & \text{for } x_1 \leq 1 \\ \frac{\frac{1}{2}(x_2^2 - 2x_1 + 1)}{x_2 - x_1} & \text{for } x_1 \geq 1. \end{cases}$$

This will be expressed in the final form by

$$\frac{M}{M_s} = \begin{cases} \frac{1}{2}(n_1 + n_2)H_e & \text{for } n_1 H_e \leq 1 \\ \frac{\frac{1}{2}(n_2^2 H_e^2 - 2n_1 H_e + 1)}{(n_2 - n_1)H_e} & \text{for } n_1 H_e \geq 1. \end{cases} \quad (3.14)$$

where

$$n_1 = -\frac{M_s}{2b_1 e} \quad \text{and} \quad n_2 = -\frac{M_s}{2b_2 e}. \quad (3.15)$$

The solution is  $M/M_s = 1$  above the magnetic field for which  $n_2 H_e = 1$ .

The predicted magnetization curve is linear until  $n_1 H_e = 1$ . (See Figure 3.5.) In this region it has the same form as obtained in the interacting grain theory,

$$\frac{M}{M_s} = -\frac{M_s}{2B_e} H_e,$$

except  $B$  is given by the arithmetic mean,

$$\frac{1}{B} = \frac{1}{2} \left( \frac{1}{b_1} + \frac{1}{b_2} \right).$$

The subsequent magnetization curve joins continuously to first and second order but approaches saturation more slowly than the interacting grain magnetization curve.

In the case of magnetoelastic isotropy ( $b_1 = b_2$ ), the independent grain theory degenerates to the predicted curve for the interacting grain theory. The predicted magnetization curves for the two assumptions along with those for the <100> and <111> problems are shown in Figure 3.5 for YIG.

### 3.3. Micromagnetic Theory

The intention in this section is to review briefly the concepts of micromagnetic theory and its progress concerning the shock induced anisotropy effect. The theory proceeds by invoking the thermodynamic equilibrium postulate on the total integral energy expression, Equation (2.15).<sup>31,47</sup> The resulting variation, accomplished by calculus of variation techniques, yields Brown's equations which, along with the corresponding magnetostatic boundary value problem, constitute a system of nonlinear differential equations for the magnetization field throughout the material parameterized on the external applied field  $H_e$ .

Since this system of equations is nonlinear, for a given  $H_e$  many solutions are allowed. Some of these solutions will be stable while others will be unstable. Each stable solution represents a possible physical state of the thermodynamic system. Which state is occupied depends on the history as well as existing conditions. Hence, this theory is capable of predicting magnetic hysteresis. With variation of the applied field  $H_e$ , the present state of the system may change continuously or by finite jumps if the state becomes unstable. These jumps are known as Barkhausen jumps and have been observed experimentally.

Progress by this very elegant approach has been limited due to the extreme complexity of the system of nonlinear equations. Some success has been made in select regions of the magnetization curve for very special geometries of magnetic material.<sup>31,47</sup>

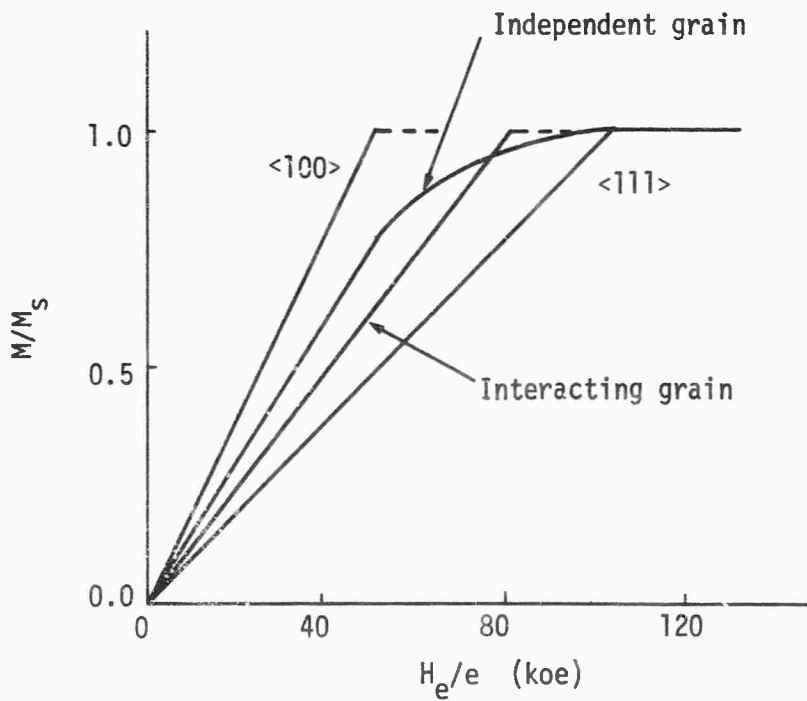


Fig. 3.5.--Magnetization curves for various theories'.

The only progress through micromagnetic theory on the shock induced anisotropy effect has been made by Bartel.<sup>11</sup> He used an alternative approach, known as the Rayleigh-Ritz method, which circumvents direct use of Brown's equations. This method assumes a form for the final solution with a sufficient number of undetermined parameters. The total energy integral is then minimized with respect to these parameters.

His development assumed a uniform anisotropy field as would occur in single crystals for specific orientations or as would occur in polycrystals under the interacting grain assumption. By approximating the argument of the energy integral expression and by considering first harmonics in the assumed Rayleigh-Ritz solution and corresponding magnetostatic potential, he was able to draw conclusions about domain size, nucleation field, and subsequent deviation from magnetic saturation.

### 3.4. Porosity Effect

Previous observations suggest that the major structural defects capable of significantly altering the results obtained in earlier sections are nonmagnetic inclusions in the form of voids or impurities.<sup>12</sup> Porosity is characteristic of magnetic ceramics. Even the best hot pressing techniques are capable of producing garnets only to about 98% or 99% theoretical density while in ferrites 95% is a good number. This is probably characteristic of natural materials also.

Experiments by Wayne et al.<sup>12</sup> show that polycrystalline magnetic ceramics, when subject to hydrostatic pressure, show a strong dependence of magnetization on pressure. Their interpretation was that nonhydrostatic strains occurring in the vicinity of cavities created local magnetic anisotropy fields which produced local deviations in the magnetization and, hence, the

observed effect. It has been suggested that this same effect might occur to some extent in the present shock induced anisotropy situation.

A calculation which relates the magnetization to the hydrostatic pressure and the porosity in the approach to saturation region of the magnetic material has been made.<sup>48</sup> This calculation is based on the assumption that the average behavior of an aggregate of cavities in the medium can be represented by the behavior of a spherical pore in an isotropic elastic continuum. The strain around a spherical pore in an isotropic elastic medium subject to external hydrostatic pressure deviates from hydrostatic strain. This deviation contributes to the anisotropy energy. The energy density at a distance  $r$  from the center of a pore of radius  $a$  has been calculated to be

$$\epsilon = \frac{3}{4} \frac{B}{\mu} P \frac{a^3}{r^3} \cos^2(\psi + \theta) - H_e M_s \cos \psi \quad (3.16)$$

where the first term is the induced anisotropy energy and the second is the interaction energy.  $\theta$  is the angle between the field point and the applied magnetic field.  $\psi$  is the angle between the magnetization at the field point and the applied magnetic field.  $\mu$  is the shear modulus and

$$B = \frac{2}{5} b_1 + \frac{3}{5} b_2.$$

Equation (3.16) is derived in Appendix IV. By numerical methods, this expression leads to a prediction of the dependence of magnetization on  $P$  and  $H_e$ . Figure 3.6 shows this magnetic dependence on  $H_e$  for 3% porous YIG at two values of hydrostatic pressure.

The intention of this section is to make a simple estimate of the effect of porosity on the shock induced anisotropy effect for slightly porous material. In particular, 3% porous YIG will be considered since this material was utilized in these studies. It will be assumed that the correction to

the predicted magnetization due to porosity is small and can be superposed on the actual strain induced anisotropy results. This correction will be obtained from the previously discussed numerical hydrostatic prediction by using, instead of the hydrostatic pressure, the mean pressure

$$\bar{P} = \frac{\sigma_x + 2\sigma_y}{3}.$$

This correction cannot be added directly but must be weighted since the full correction is realized only when the material is initially in magnetic saturation. In fact, when the strain induced anisotropy predicts

$$\frac{M}{M_s} = \frac{\pi}{4},$$

the correction will be zero since this is exactly the average value of  $\cos\psi$

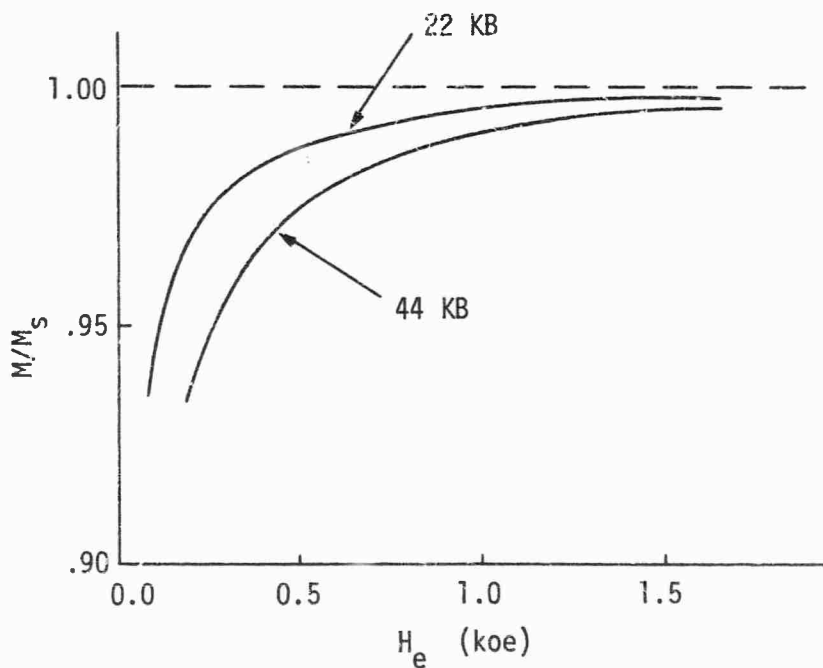


Fig. 3.6.--Magnetic hydrostatic pressure dependence of 3% porous yttrium iron garnet.

distributed around a spherical pore. Thus, the magnetization will be

$$\frac{M}{M_s} = f(e, H_e) + w(M/M_s) \Delta(\bar{P}, H_e)$$

where  $f(e, H_e)$  is the strain induced anisotropy prediction (Equation (3.12) for the interacting grain theory and Equation (3.14) for the independent grain theory),  $\Delta(\bar{P}, H_e)$  is the full numerical porosity correction, and  $w(M/M_s)$  is the weight factor. The correction is assumed to be small so a linear approximation of  $w(M/M_s)$  will be used. Since

$$w(1) = 1$$

and

$$w(\pi/4) = 0,$$

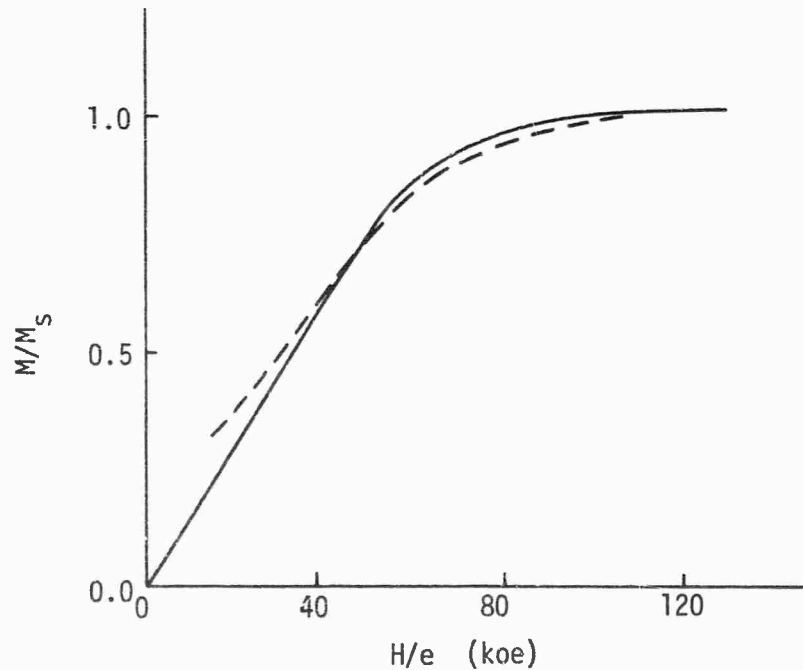


Fig. 3.7.--Correction to independent grain assumption due to 3% porosity.

one obtains

$$\frac{M}{M_s} = f(e, H_e) + \frac{\left(\frac{M}{M_s} - \frac{\pi}{4}\right)}{\left(1 - \frac{\pi}{4}\right)} \Delta(\bar{P}, H_e). \quad (3.17)$$

The correction is shown in Figure 3.7 for the independent grain assumption. This correction is seen to be negligible in the higher regions of the magnetization curve and obtains significance only in the lower part of the curve where the applied field is substantially lower. It is important to notice that for large strains the effect of porosity on the magnetization curve becomes quite significant. This is believed, by Royce, to explain the shock demagnetization results of Shaner and Royce<sup>8</sup> in the plastic region of YIG. Shock pressures of 90 to 440 kbars were obtained in that work.

## CHAPTER IV

### EXPERIMENTAL METHOD

An experimental design should reproduce as closely as possible the requirements of the theoretical model. These requirements are an infinite slab of ferromagnetic material in a state of uniaxial strain normal to the plane of the slab and an applied magnetic field in the plane of the slab. Experimentally, the infinite slab of ferromagnetic material was approximated by a rectangular slab of yttrium iron garnet, YIG. The state of uniaxial strain was obtained by planar impact of a projectile from a four inch gas gun. The magnetic field was applied by a pulsed current through a rectangular solenoid enveloping the specimen. A schematic representation of the experimental procedure is illustrated in Figure 4.1. This will hopefully aid in correlating details with the overall experimental design.

Briefly, the experimental sequence is as follows. A projectile traveling at a velocity  $\vec{v}$  triggers a current supply. The subsequent current produces a magnetic field which reaches a maximum at the time the projectile impacts the target. The impact produces a strain wave which propagates through the solenoid and into the YIG sample. This sample, initially in magnetic saturation, is demagnetized by the strain wave. The demagnetization develops an emf across the pickup coil which is recorded on the monitoring oscilloscopes. The magnetic equation of state of the ferromagnetic material behind the shock front is determined from these records.

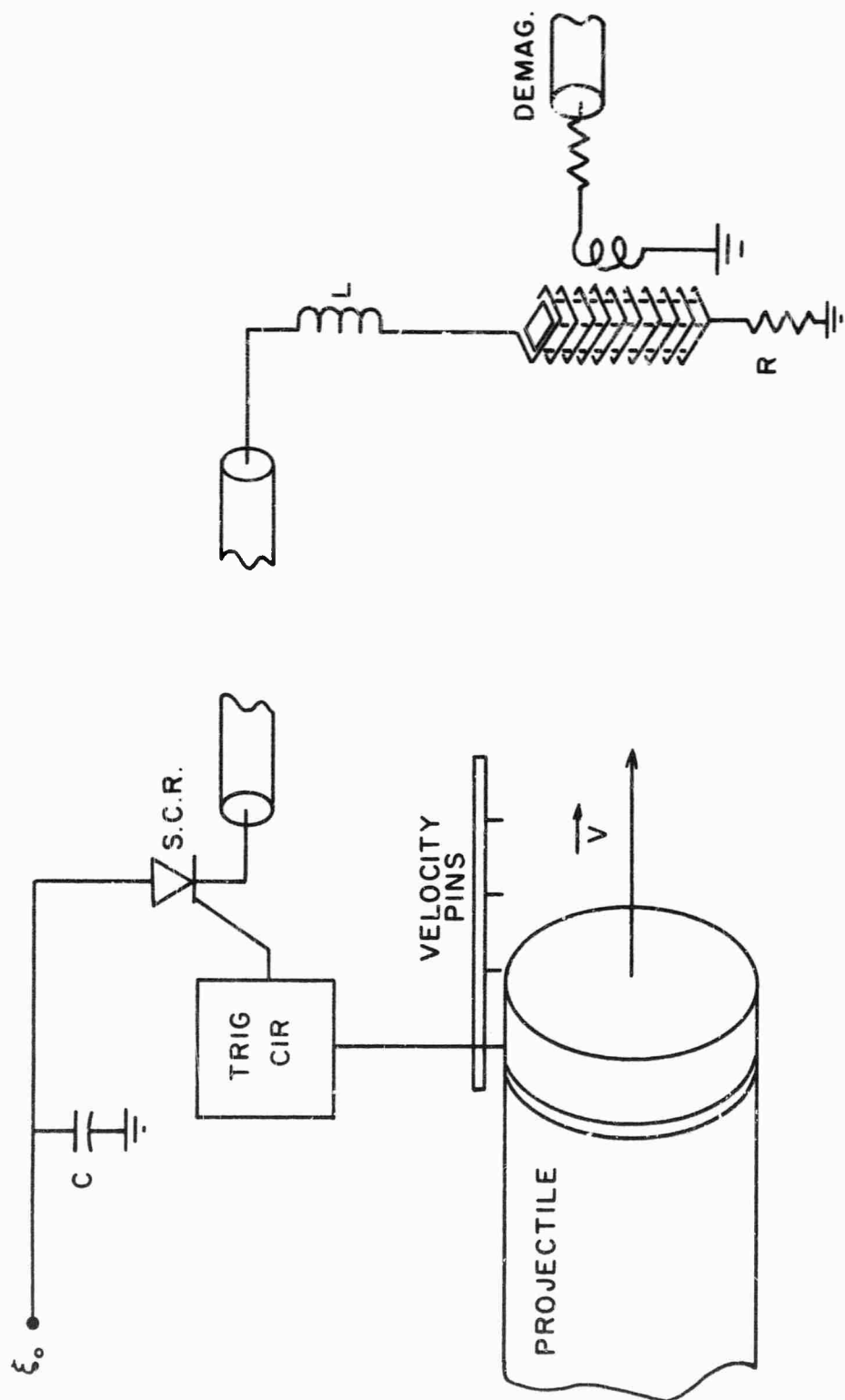


Fig. 4.1.--Schematic representation of experimental method.

#### 4.1. Application of Magnetic Field

The objective is to create a magnetic field by driving a large current pulse through a rectangular solenoid coincident in time with the application of the strain field. Referring to Figure 4.2, the operation is as follows. A large electrolytic capacitor,  $C$ , is charged to a predetermined voltage,  $\varepsilon_0$ . At a predetermined time prior to application of the strain field the silicon control rectifier is triggered. Capacitor  $C$  then discharges via high voltage cables through the solenoid at a rate determined by the  $L$ ,  $R$ , and  $C$  of the circuit. A current pulse of the form

$$I(t) = \frac{\varepsilon_0}{\omega L} e^{-\beta t} \sinh \omega t$$

is obtained where

$$\beta = \frac{R}{2L}$$

and

$$\omega = \left( \frac{R^2}{4L^2} - \frac{1}{LC} \right)^{1/2}.$$

Preadjustment of  $\varepsilon_0$ ,  $R$ , and  $L$  allows a predetermined current  $I_{max}$  to be attained at a predetermined time  $\tau_m$  governed by

$$\tanh \omega \tau_m = \frac{\omega}{\beta}.$$

This time is adjusted so that the shock wave passes through the specimen when  $I = I_{max}$ . The transit time is approximately  $0.25 \mu s$ . The current is essentially steady during this time. The time variation in the neighborhood of  $\tau_m$  is

$$\frac{\Delta I}{I} \approx \frac{1}{2LC} (t - \tau_m)^2.$$

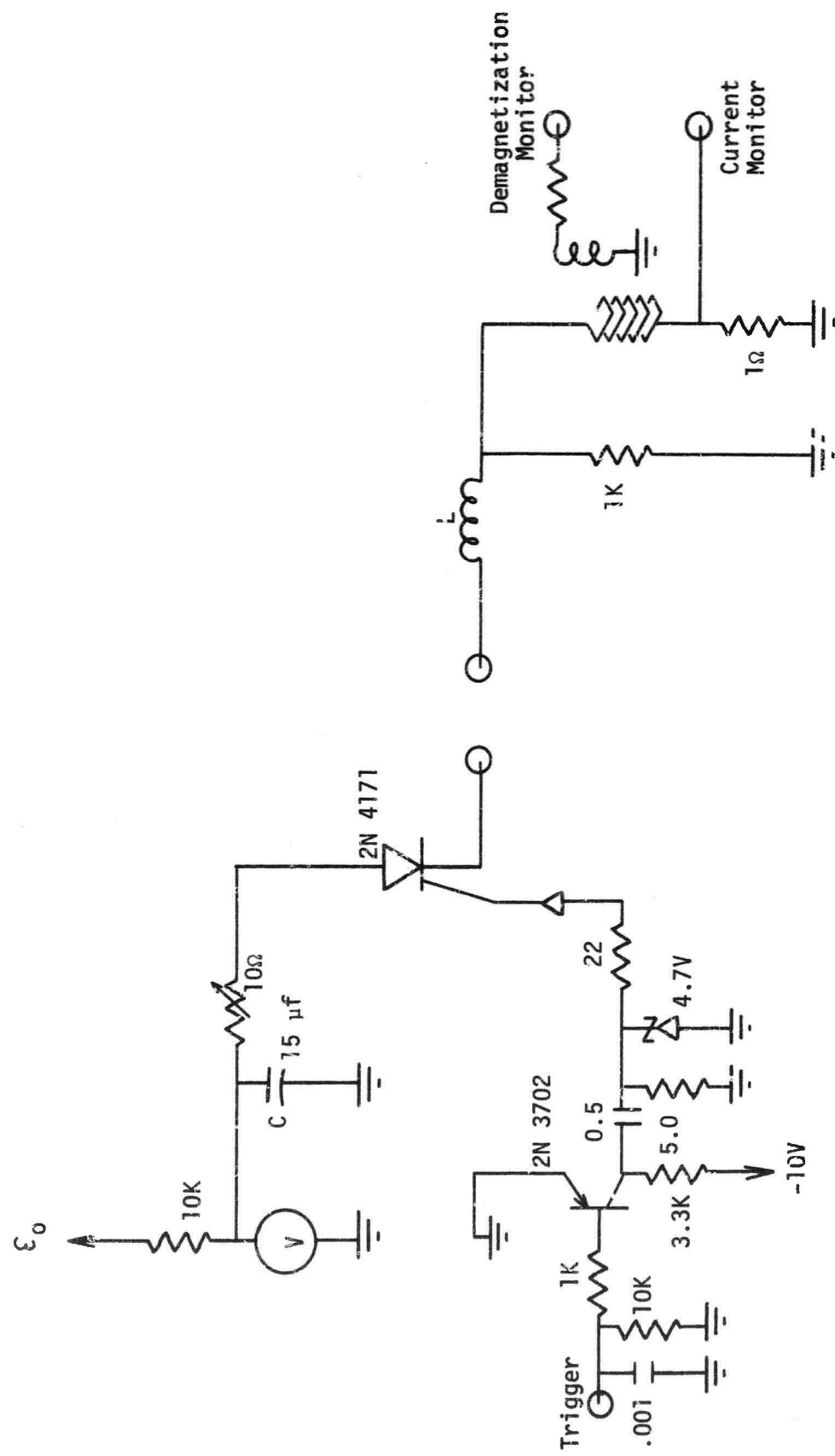


Fig. 4.2.--Current supply and target circuit.

For the chosen components, this fluctuation is about 0.01% for the required recording time.

The inductor  $L$  is an integral part of the experimental design. It is, of course, a major component in determining the rise time of the current pulse. More important, the inertia of the inductor maintains the current and, therefore, the applied magnetic field constant for the duration of the experiment. There are several effects which attempt to change the current. First, passage of a shock wave across the solenoid accelerates the forward face creating an effective solenoid collapse. Electromotive forces are generated in an attempt to produce currents which would conserve the flux in the closing solenoid area and thus increase the magnetic field. Second, when the stress wave transverses the magnetic sample, a gross flux reduction occurs. The response of the electric circuit is to attempt to compensate for this flux change. In both cases, it is the responsibility of the inductor  $L$  to maintain the current constant, denying the natural response of the system. About 0.25 to 0.5 millihenry inductors have been found sufficient for this purpose. It should be mentioned that this inductor is physically located within a few inches of the solenoid since its inertial characteristics must be realized within nanoseconds. To locate this inductor in the current supply would create coaxial cable reflections and nullify its stabilizing property.

There is a  $1,000\Omega$  resistor paralleling the solenoid to ground. This resistor carries several percent of the total current and, with the solenoid, has an  $L/R$  time sufficient to damp out ringing due to the finite stray capacitance of the solenoid windings.<sup>49</sup>

The current through the solenoid is monitored by recording the voltage across a precision  $1\Omega$  resistor in series with the solenoid as shown in Figure 4.2. The magnetic field is given by the solenoid formula

$$H_e = 0.4\pi NI \quad (4.1)$$

where  $I$  in amperes and  $N$  in turns per centimeter gives the magnetic field in oersteds.

The solenoid is constructed of 1 by 15 mil (1 mil = .001 inches) OFHC copper ribbon obtained from The Wilkenson Co.<sup>50</sup> Usually between 12 and 20 turns per centimeter were used. The solenoid constituted about 6 to 9Ω of D.C. resistance, a factor which must be considered in the total circuit design. A standard lathe, set in the thread cutting mode, was found to provide an efficient and versatile means for winding a very smooth and regular solenoid. Magnetic fields required for this work required currents up to 60 amperes. The joule heating during pulsing was still substantially less than the softening temperature of epoxy; approximately 80°C.

A problem of concern is the ripple in the magnetic field due to the finite spacing of the solenoid windings. The magnitude is estimated by the following method. In the neighborhood of the grid, the magnetic vector potential is periodic and can be written as a superposition of terms,

$$\vec{A}_n = \vec{A}_n(y) \cos \frac{2n\pi x}{a},$$

where  $y$  is the normal direction from the grid,  $x$  is along the grid, and  $a$  is the period of the grid. The vector potential must satisfy Laplace's equation. Hence,

$$\frac{d^2 \vec{A}_n(y)}{dx^2} - \frac{4n^2 \pi^2}{a^2} \vec{A}_n(y) = 0,$$

which has the solution

$$\vec{A}_n(y) = \vec{A}_n e^{-2n\pi y/a}.$$

The first harmonic is reduced by  $1/e$  in a distance

$$y_0 = \frac{a}{2\pi},$$

while higher harmonics fall off even faster. Therefore, ripple in the magnetic field is less than 1% at a distance from the grid equal to the period of the grid. In this case, it is about 20 to 30 mil.

Another problem is the end effect or reduction in the magnetic field due to the finite length of the solenoid. For a rectangular solenoid of dimensions  $b$  and  $c$  with  $c > b$ , the end effect error is

$$\frac{H_I - H_e}{H_I} = \frac{1}{2} - \frac{1}{\pi} \tan^{-1} \frac{x}{b}, \quad (4.2)$$

where  $H_e$  is the actual field,  $H_I$  is the infinite solenoid field, and  $x$  is the distance into the solenoid from the end. The solenoid must be constructed sufficiently long to nullify this error in the region of the specimen.

#### 4.2. Application of Strain Field

The strain field required in the magnetic sample was produced by planar impact of a projectile accelerated in a four inch gas gun.<sup>51</sup> The sample, solenoid, and required electronics are assembled in a target which is mounted at the muzzle end of the gas gun. This in turn, is enclosed in an evacuated target chamber. Impact tiles are characteristically on the order of  $10^{-4}$  radians.

##### 4.2.1. Experimental Construction

The normal metal faces of the projectiles were replaced by nonconducting material, usually Lucite or a ceramic such as aluminum oxide, in order to eliminate moving metal from the vicinity of the solenoid and, hence, reduce gross movement of magnetic flux during the experiment. The velocity of the

projectile is measured by contact pins prior to its arrival at the target face. This is required for determining the final state of strain in the YIG. The velocity contact pins also serve to trigger the current supply.

The target is constructed so that the plane wave propagates through the solenoid and then into the YIG. See Figure 4.3. Materials through which the wave travels between projectile and YIG are, in order, 0.75 millimeters of Lucite, 0.025 millimeters of alternate copper and epoxy, 0.75 millimeters of Lucite, and 0.025 millimeters of epoxy which includes the front face of the pickup coil. All electronic components are mounted behind the solenoid assembly and are completely potted in epoxy.

There are several problems associated with propagating a planar shock wave through the periodic grid defined by the front surface of the solenoid.

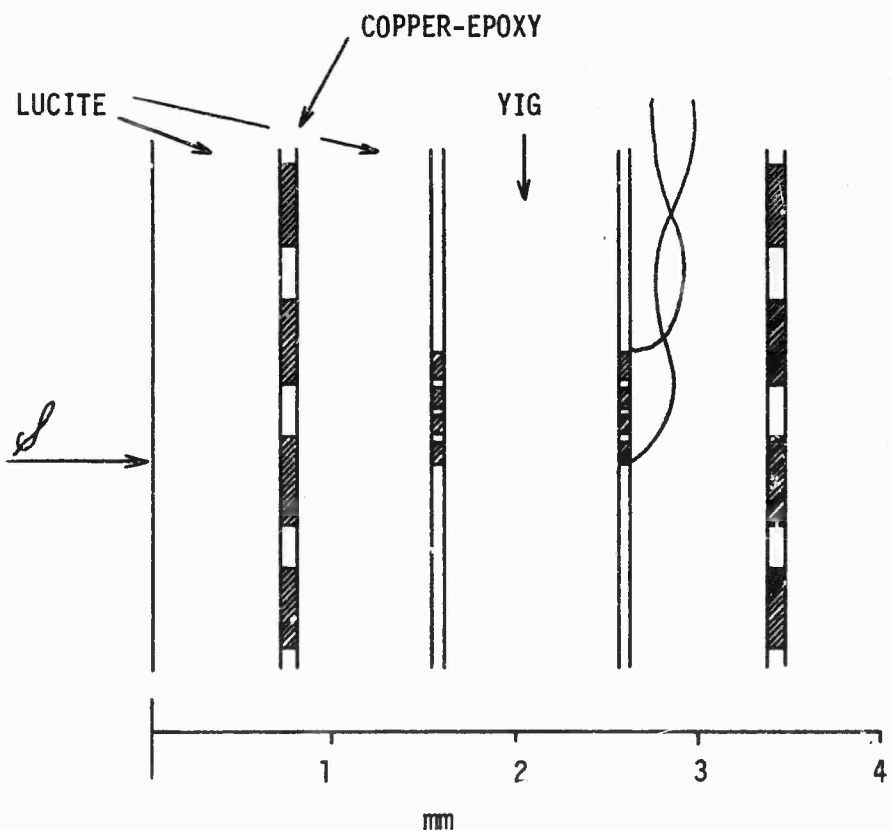


Fig. 4.3.--Solenoid construction.

First, the copper-epoxy interface is a region of mechanical impedance mismatch through which the wave must travel. The resulting ringup in this region degrades the wave and lends a finite rise time to an initial step stress wave. A volume average density for the grid region predicts approximately a 50 nanosecond risetime for the stress profile. Quartz gauge records have verified this prediction. Second, the periodicity of the grid creates a corrugated wave effect due to the differing velocities and impedances in the grid materials. This effect will diminish with propagation distance from the grid due to Huygen's principle and due to nonlinearity and viscosity of the Lucite.

Mineev et al.<sup>52</sup> have shown that in metals at high pressures the perturbation amplitude (in this case several times the grid thickness) drops to a small amount in less than several times the period of the grid. It has been assumed that this problem does not significantly affect the experimental results.

A technique capable of virtually eliminating the problems associated with the solenoid grid was invented while this work was in progress. The method requires simply replacing the first region of Lucite in Figure 4.3 with an aluminum oxide ceramic. The stress wave then propagates through aluminum oxide, the copper-epoxy grid, and Lucite, respectively. The material characteristics which make this technique successful are the mechanical impedance similarities of aluminum oxide and copper on one hand and Lucite and epoxy on the other along with the similar shock velocities of copper and epoxy. This peculiar combination of properties essentially creates a single interface of a somewhat ragged nature. An experiment was performed in which two quartz gauges analyzed waveforms propagating through identical geometries with the exception that one contained a copper-epoxy grid while the other did not. The waveforms were identical. A similar set of circumstances exists at the interface containing the pickup coil. This explains why no deteriorating effects are observed due to it.

#### 4.2.2. Equation of State

The state of strain in the YIG was obtained in two ways. First, by use of measured projectile velocities, calculations through the intermediate materials into the YIG were made. Second, quartz gauge techniques were used.<sup>53</sup> In each case, equation of state information for the various materials involved was required.

A linear elastic equation of state was assumed for the YIG. This information has been collected, along with other required physical properties of YIG, in Table 2.

An aluminum oxide ceramic, Wesgo 995,<sup>54</sup> was used as a projectile face material. It was assumed to be linear elastic. The equation of state parameters used were<sup>55</sup>

$$D = 1.03 \text{ cm}/\mu\text{s},$$

$$V_0 = 0.2615 \text{ cc/g}, \quad (4.3)$$

and

$$Z = 3.939 \text{ mB}(\text{cm}/\mu\text{s})^{-1}.$$

The Lucite used was Rohm and Haas, Type G. The material, obtained in 30 mil sheets, had a specific volume of 0.847 cc/g. A cubic P - u relation,

$$P = 0.336u + 1.12u^2 + 5.11u^3, \quad (4.4)$$

was fit by the method of least squares to data by Liddiard<sup>56</sup> and Barker and Hollenbach<sup>57</sup> in the region of 0 to 60 kilobars. The units are megabars, centimeters, and microseconds.

The stress wave at the Lucite-YIG interface undergoes a reflection with a jump in stress. To calculate this final stress state requires

knowledge of the recentered Hugoniot in the Lucite. To obtain this recentered Hugoniot, a Mie-Grüneisen equation of state was assumed in the Lucite.<sup>58</sup> When referenced from the foot of the initial Hugoniot, this takes the form

$$\begin{aligned} P(V, E) &= P(S_0, V) + \frac{\Gamma}{V} (E - E(S_0, V)) \\ &= \frac{\Gamma}{V} (E - E(S_0, V_0)) + P(S_0, V) + \frac{\Gamma}{V} \int_{V_0}^V P(S_0, v) dv. \end{aligned}$$

Collecting the volume-dependent-only terms into an arbitrary function gives

$$P(V, E) = \frac{\Gamma}{V} (E - E(S_0, V_0)) + f(V). \quad (4.5)$$

The energy jump condition on the initial Hugoniot is

$$E - E(S_0, V_0) = \frac{1}{2} P_H^0 (V_0 - V). \quad (4.6)$$

Equation (4.5) must hold in particular on the initial Hugoniot. Therefore, by eliminating the energy expression between Equation (4.5) and Equation (4.6), one obtains

$$P_H^0 (V) = \frac{\Gamma}{2V} P_H^0 (V_0 - V) + f(V).$$

Solving this for  $f(V)$  and substituting back into Equation (4.5) gives the required Mie-Grüneisen equation of state,

$$P(V, E) = \frac{\Gamma}{V} (E - E(S_0, V_0)) + P_H^0 (V) \left( 1 - \frac{\Gamma}{2V} (V_0 - V) \right).$$

The energy jump condition on the recentered Hugoniot is

$$E - E' = \frac{1}{2} (P_H - P') (V' - V),$$

where  $P' = P_H^0(V')$  and  $(P', V')$  represent the reference state for the recentered Hugoniot. When combined with the energy jump condition on the initial Hugoniot, this gives

$$E - E(S_0, V_0) = \frac{1}{2} P'(V_0 - V') + \frac{1}{2} (P_H + P')(V' - V).$$

Combining this with the Mie-Grüneisen equation of state gives the required pressure on the recentered Hugoniot.

$$P_H(V) = \frac{P_H^0(V) \left[ 1 - \frac{\Gamma_0}{2} \frac{V_0}{V} \left( 1 - \frac{V}{V_0} \right) \right] + P' \frac{\Gamma}{2} \frac{V_0}{V} \left( 1 - \frac{V}{V_0} \right)}{1 - \frac{\Gamma_0}{2} \frac{V_0}{V} \left( \frac{V'}{V_0} - \frac{V}{V_0} \right)} \quad (4.7)$$

To facilitate the calculation, a quadratic  $P - \eta$  relation,  $\eta = 1 - V/V_0$ , was fit to the initial Hugoniot data in the range 10 to 60 kilobars. The result,

$$P_H^0(\eta) = 0.0197 - 0.223\eta + 1.51\eta^2, \quad (4.8)$$

was not forced through the origin. This allowed a better fit to the data in the region of interest. The quantity  $\Gamma/V$  was assumed constant. The value of  $\Gamma_0$  is difficult to assess from the literature. Acoustical data<sup>59</sup> give  $\Gamma_0 = 5.13$  while thermodynamic data<sup>60</sup> predict  $\Gamma_0$  approximately equal to 0.9. A gross linear fit to  $D - u$  data, using the relation<sup>61</sup>

$$\Gamma_0 = 2 \frac{dD}{du} - 1,$$

yields a value of  $\Gamma_0 \approx 0.8$ . For this work, strains using a value of  $\Gamma_0 = 1.0$  are quoted. In practice, pressures of about 22 kilobars and 44 kilobars were obtained in the Lucite. Predictions of strain for  $\Gamma_0 = 5.13$  are 1% and 4% lower, respectively.

### 4.3. Demagnetization Measurement

The reduction in magnetization is measured by recording the flux change in a pickup coil surrounding the sample of yttrium iron garnet. This pickup coil consists of 10 turns of 1 mil by 15 mil manganin ribbon wound intimately around the specimen as shown in Figure 4.3. The active recording region, defined by the face of the pickup coil, is about  $1 \text{ cm}^2$ . Manganin ribbon was originally chosen because of its distributed resistance. It was thought that this resistance might tend to dampen parasitic oscillations in the pickup circuitry. No attempt has been made to test the merit of this precaution. The pressure dependence of the resistance is negligible for this experimental configuration. A twisted pair of 3 mil, insulated copper wires are solder-connected to the pickup coil immediately behind the YIG sample and brought out the end of the solenoid. This twisted pair and their connections are not disturbed by the stress wave during the recording time.

A high impedance recording circuit is used to monitor the emf developed across the pickup coil during the demagnetization process. The equivalent circuit, shown in Figure 4.4, consists of an ideal source of emf and a resistance  $R$  consisting of the load resistance plus the internal resistance of

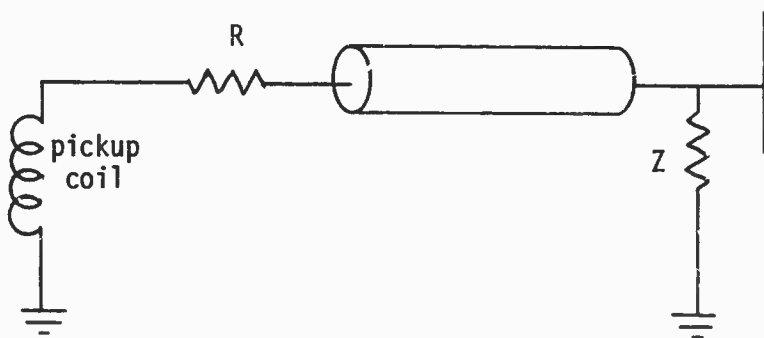


Fig. 4.4.--Pickup coil circuit.

the pickup coil. The signal is transmitted to the recording oscilloscope by  $50\Omega$  coaxial cable and terminated there in  $50\Omega$ . The emf is given by

$$\epsilon(t) = \frac{(R + Z)}{Z} V(t) \quad (4.9)$$

where  $V(t)$  is the voltage recorded at the monitoring oscilloscope and  $Z$  is the characteristic impedance of the coaxial cable. The resistance  $R$  is selected to maintain the current flow in the pickup circuit sufficiently small such that the magnetic field produced by this current is negligible compared to the magnetic field produced by the solenoid. In practice, several hundred ohms are found to be sufficient for this purpose. The dynamic impedance of the pickup coil inductance is small compared to this resistance.

To relate the demagnetization to the emf developed, it will be assumed that a steady state shock profile is progressing through the magnetic material as shown in Figure 4.5. In the spirit of mechanical jump condition calculations,<sup>58</sup> consider, prior to passage of the shock wave, an element of area  $bD\delta t$  which is compressed to  $b(D - u)\delta t$  after passage of the shock wave.  $b$  is the width of the pickup coil and  $D$  is the velocity of the shock profile. The change in magnetic flux across the shock wave is

$$\delta\Phi = b(B(D - u) - B_0 D)\delta t$$

where  $B_0$  is the initial magnetic induction and  $B$  is the final magnetic induction. Considering the case where the external applied field is constant and using

$$B = H_e + 4\pi M$$

along with the jump condition,

$$(D - u)\rho = D\rho_0,$$

one obtains

$$\delta\Phi = bD \left[ 4\pi \left( M \frac{\rho_0}{\rho} - M_0 \right) + \left( \frac{\rho_0}{\rho} - 1 \right) H_e \right] \delta t,$$

where  $M_0$  is the initial magnetization per unit initial volume and  $M$  is the final magnetization per unit final volume. Since

$$D \left( \frac{\rho_0}{\rho} - 1 \right) = -u$$

and  $M_0/\rho$  is the final magnetization per unit initial volume, the rate of flux change becomes

$$\frac{d\Phi}{dt} = 4\pi b D \delta M - bu H_e. \quad (4.10)$$

The first term is the change in flux due to the reduction in magnetization.

The second term is the flux change due to motion of the front surface of the

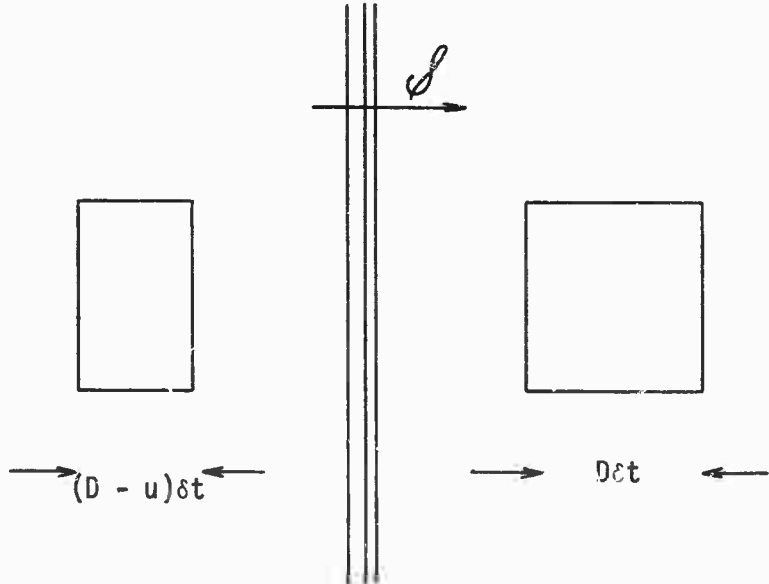


Fig. 4.5---Geometry for magnetic flux jump condition. Area compression due to shock propagating into medium at rest is represented. Magnetic field is normal to the page.

pickup coil in the manner of a magnetic velocity gauge. When the latter can be neglected,

$$\frac{d\Phi}{dt} = 4\pi b D \delta M. \quad (4.11)$$

Faraday's Law

$$\mathcal{E} = 10^{-8} N \frac{d\Phi}{dt} \quad (4.12)$$

relates the induced emf in volts to the turns in the pickup coil and the flux in gauss-cm<sup>2</sup>-sec<sup>-1</sup>. From this, one finally obtains

$$\begin{aligned} \delta M &= \frac{10^8}{4\pi b ND} \mathcal{E} \\ &= \frac{10^8}{4\pi b ND} \frac{R + Z}{Z} V. \end{aligned} \quad (4.13)$$

Thus, for a steady state shock wave, the induced emf is constant and is proportional to the demagnetization.

#### 4.4. Material

The material selected for this study was hot pressed polycrystalline yttrium iron garnet.<sup>62</sup> It was chosen because the magnetoelastic properties are of convenient magnitude for experimental investigation. This was also the same material used by Shaner and Royce<sup>8</sup> in earlier investigation of the shock induced demagnetization effect at higher stresses. The following paragraphs will present the material characterization performed during this work.

Photomicrographs were obtained of polished sample surfaces. A uniform distribution of highly spherical pores, characteristic of sintered ceramics, was observed. The pore diameters ranged from 1 to 3 microns. There was some evidence of other inclusions.

TABLE 2.--Material properties of single crystal yttrium iron garnet

Property	Source	Values
Second order elastic moduli	a	$c_{11} = 2.69 \times 10^{12}$ dyn/cm <sup>2</sup> $c_{12} = 1.08 \times 10^{12}$ dyn/cm <sup>2</sup> $c_{44} = 0.76 \times 10^{12}$ dyn/cm <sup>2</sup>
First order magneto-elastic constants	b	$b_1 = 3.5 \times 10^6$ erg/cm <sup>3</sup> $b_2 = 6.9 \times 10^6$ erg/cm <sup>3</sup>
Second order magneto-elastic constants	b	$B_{111} = 173 \pm 12 \times 10^6$ erg/cm <sup>3</sup> $B_{123} = 22 \pm 19 \times 10^6$ erg/cm <sup>3</sup> $B_{144} = -5 \pm 41 \times 10^6$ erg/cm <sup>3</sup> $B_{155} = -37 \pm 5 \times 10^6$ erg/cm <sup>3</sup> $B_{441} = -24 \pm 14 \times 10^6$ erg/cm <sup>3</sup> $B_{456} = -27 \pm 7 \times 10^6$ erg/cm <sup>3</sup>
Crystal anisotropy constant	c	$K_1 = -6.2 \times 10^3$ erg/cm <sup>3</sup>
Saturation magnetization at T = 293°K	c	$M_s = 133.7$ gauss
Ne'el temperature	d	$T_N = 563^\circ K$
Pressure dependence of Ne'el temperature	d	$\partial T_N / \partial P = 1.25^\circ K \text{ kbar}^{-1}$
Temperature dependence of saturation magnetization at T = 293°K	e	$\frac{1}{M_s} \frac{\partial M_s}{\partial T/T_N} = -0.61$

TABLE 2--Continued

Property	Source	Values
Theoretical density	f	$\rho_0 = 5.17 \text{ g/cm}^3$
Lattice constant	f	$a_0 = 12.38 \text{ \AA}$
Longitudinal velocity (polycrystalline)	g	$D = 7.17 \text{ mm/\mu s}$
Coefficient of expansion	f	$\alpha = 1.39 \times 10^{-5} \text{ }^\circ\text{K}^{-1}$
Isothermal compressibility	g	$K_T = 6.1 \times 10^{-4} \text{ kbar}^{-1}$
Specific heat	h	$C_V = 0.162 \text{ cal/gm deg}$

<sup>a</sup>T. B. Bateman, J. Appl. Phys. 37, 2194 (1966).

<sup>b</sup>D. E. Eastman, Phys. Rev. 148, 530 (1966) and references contained therein.

<sup>c</sup>Handbook of Microwave Ferrite Materials, W. H. vonAuack, Ed. (Academic Press Inc., New York, 1965), and references contained therein.

<sup>d</sup>D. Bloch, F. Chaissé, and R. Pauthenet, J. Appl. Phys. 37, 1401 (1966).

<sup>e</sup>Estimated from Pauthenet, Ann. de Phys. 3, 425 (1958).

<sup>f</sup>S. Geller and M. A. Gilleo, J. Phys. Chem. Solids 3, 30 (1957).

<sup>g</sup>A. E. Clark and R. E. Strakna, J. Appl. Phys. 32, 1172 (1961).

<sup>h</sup>Calculated from Dulong and Petit limit.

Photomicrographs were made of fracture surfaces. The average grain size was found to be approximately 15 microns with a distribution of from 5 to 25 microns. The grain distribution was homogeneous throughout the sample. The grain distribution appeared visually isotropic; that is there was no evidence of mechanical texture created by the hot pressing process. The pores were observed to occur both intragranularly and at grain boundaries.

The porosity of the material was obtained by measuring and weighing rectangular samples, by liquid displacement, and by analysis of photomicrographs. The porosity obtained was  $3.3 \pm 0.5\%$  where the theoretical density from Table 2 was used.

A spectrographic analysis for metallic impurities was performed. The results are shown in Table 3. Tests for organic inclusions or oxygen impurities were not made.

TABLE 3.--Spectrographic analysis for metallic impurities

Element	Percent
Fe	Principle constituent
Y	Principle constituent
Ca	.05
Si	.01
Al	.01
Ni	.01
Cr	.01
Mg	.005
Ag	.003
Mn	.002
Cu	.0005

The samples were received as rectangular slabs of dimensions 0.1 x 1.0 x 5.0 cm. The specimens were lapped flat and parallel with #1700 aluminum oxide lapping compound.

The saturation magnetization of the material was determined by magnetizing several samples from zero magnetization to some value determined by the final magnetic intensity. This was performed by initially demagnetizing the specimen and then pulsing a current through the solenoid enveloping the specimen. The data provided a linear plot which was fit to the Weiss relation,<sup>63</sup>

$$M = M_s \left( 1 - \frac{a}{H} \right). \quad (4.14)$$

$M_s$  and  $a$  were obtained from the intercept and the slope. The saturation magnetization obtained was about 124 gauss. The theoretical value (see Table 2), reduced by the amount expected due to the porosity of the material, is 128 gauss. The latter value was used due to the author's lack of confidence in the somewhat painfully obtained first value.

The magnetoelastic constants  $b_1$  and  $b_2$  were not measured. The constants used (see Table 2) were most probably values obtained from the literature.

#### 4.5. Experimental Corrections

This section will address various experimental perturbations and considerations which will affect, to some degree, the ideal measurement presupposed. The first few problems are related to the experimental design; others concern material behavior.

Since the rectangular specimen is of finite length, there will be an additional contribution to the magnetic field created by the magnetic poles at the end faces. An exact calculation of this field would be very difficult.

However, an approximate value can be obtained by considering the specimen end faces as point magnetic poles of charge,

$$Q_m = \pm MA,$$

where  $M$  is the magnetization and  $A$  is the area. From this, one obtains a demagnetizing field

$$H_d = -\frac{8A}{a^2} M,$$

where  $a$  is the length of the sample. This can be written

$$H_d = -DM,$$

where

$$D = \frac{8A}{a^2}$$

is the demagnetizing factor for this geometry. The maximum value for this field is about 5 oe which is approximately 2.5% of the lowest applied fields used.

In section 4.1, it was reported that the principle purpose of the large inductor was to maintain the current constant during the shock induced demagnetization process. Arbitrarily large  $L$  cannot be used since this would require a correspondingly large current supply to drive it. A sufficient value for this inductor can be obtained from the following consideration. The current fluctuation,  $\Delta I$ , produced by the shock induced emf,  $\epsilon'$ , developed across the solenoid can be obtained from

$$L \frac{d}{dt} \Delta I + \Delta I R = \epsilon'$$

with the initial condition

$$\Delta j(0) = \frac{\epsilon'}{L}.$$

The shock induced emf,  $\epsilon'$ , is on the order of

$$\epsilon' = 4\pi 10^{-8} b N D \delta M$$

where  $N$  is the number of turns in the solenoid. This has the solution

$$\Delta I = \frac{\epsilon'}{L} t \text{ for } t \ll \frac{L}{R}.$$

Thus, if  $\tau$  is the shock wave transit time, it will be sufficient to maintain

$$\Delta I = \frac{\epsilon' \tau}{L}$$

small compared to the initial current in the solenoid. In practice, 250 to 500  $\mu$ H have been found to be adequate. It should be noted that this effect tends to increase the field and is in opposition to the demagnetizing field effect.

Passage of the stress wave across the front face of the pickup coil accelerates this face creating an effective magnetic velocity gauge. Its motion produces an emf which is superimposed on the emf produced by demagnetization. This emf is given by

$$\epsilon'' = 10^{-8} N b u H_e, \quad (4.15)$$

where  $u$  is the velocity,  $b$  is the width of the pickup coil, and  $N$  is the number of turns in the pickup coil. The emf of interest, Equation (4.13), is

$$\epsilon = 10^{-8} N b D 4\pi \delta M.$$

The fractional ratio of the two is

$$\frac{\epsilon''}{\epsilon} = \frac{uH_e}{D(4\pi\delta M)},$$

which is not negligible at the lower  $\delta M$  values and must be corrected for.

It is assumed that prior to entrance of the shock wave the material is in a state of magnetic saturation. This is not, in fact, the case for a given applied field  $H$ . The actual magnetization can be roughly obtained from the Weiss relation,

$$\frac{M}{M_s} = 1 - \frac{a}{H}.$$

For this material a value of  $a = 3.6 \pm .5$  oe was obtained. This correction reaches a magnitude of 2% for the lowest magnetic fields used.

Experimentally the measured value of  $\delta M$  will be less than that predicted by Equation (3.12) and Equation (3.14) for the theoretically dense material. This is due to the porosity of the material. This correction is not concerned with the effect of porosity on the strain field. It is simply that void regions are nonmagnetic and are not contributing to the effect. This is the same correction which reduces the saturation magnetization,  $M_s$ , from the theoretical value. To be accurate, one should distinguish between the expressions for the theoretically dense material ( $M_s^{th}$ ,  $\delta M_s^{th}$ ) and the porous material ( $M_s^{por}$ ,  $\delta M_s^{por}$ ). Then the theoretical prediction of  $\delta M_s^{th}/M_s^{th}$  can be related to the measured value of  $\delta M_s^{por}/M_s^{por}$  through

$$\frac{\delta M_s^{por}}{M_s^{por}} = \frac{\delta M_s^{th}}{M_s^{th}}. \quad (4.16)$$

This distinction has not been made in the text but is implicit wherever experiment and theory are compared.

As has been previously mentioned in Chapter II, the correction due to finite strain could be substantial since the shock induced strains obtained in this work are three orders of magnitude larger than strains which occur in magnetostrictive processes. This is considered exhaustively in Appendix III.

Becker-Doring terms, as were derived in Chapter II, are terms in the magnetoelastic energy expression which are quartic in the direction cosines of the magnetization vector. These terms are seldom found to be of significance. Good values do not exist for YIG. The Becker-Doring terms can probably be safely ignored and this has been done in the present work.

The saturation magnetization is temperature dependent and will be subject to change by the adiabatic shock compression. The isentropic temperature change,

$$\Delta T = \frac{\alpha V_0 T_0}{C_p} \Delta P,$$

is calculated to be about  $2.5^{\circ}\text{K}$  and  $5^{\circ}\text{K}$  for shock strengths of 20 kbar and 40 kbar, respectively. The saturation magnetization temperature dependence from Table 2,

$$\frac{1}{M_s} \frac{\partial M_s}{\partial T/T_N} = -0.61,$$

predicts changes of  $-0.25\%$  and  $-0.5\%$ , respectively, for  $M_s$ .

The exchange interaction and hence the saturation magnetization also depends on pressure. Assuming a law of corresponding states,<sup>12</sup>

$$M_s(T)/M_s(0) = f(T/T_N),$$

taking a pressure derivative, and using values from Table 2, one can obtain

$$\frac{1}{M_s} \frac{\partial M_s}{\partial P} = 0.76 \times 10^{-3} \text{ kbar}^{-1}.$$

This is a correction of +1.5% and +3% for 20 kbar and 40 kbar, respectively. The correction is of the opposite sign from the temperature correction.

It has been observed that the magnetoelastic constants are functionally related to the saturation magnetization under a temperature variation. For instance, in nickel  $\lambda_s$  is proportional to  $M_s^2$ .<sup>46</sup> This is probably true for pressure variations. Since the material property relating the magnetization to  $H_e/e$  is a quotient of the saturation magnetization and a magnetoelastic constant, the error produced by temperature and pressure effects will be even smaller than predicted in the previous paragraphs.

## CHAPTER V

### ANALYSIS OF EXPERIMENTAL DATA

The analysis used for a systematic reduction of the experimental data is considered in this chapter. Determination of the applied magnetic field is discussed first. Next is the calculation required to estimate the state of strain in the magnetic sample from the directly measured mechanical parameters. Following this is the technique used to consistently determine the state of magnetization in the shocked ferromagnet from the actual induced emf oscilloscope records. Lastly, the experimental data resulting from this work are presented.

#### 5.1. Magnetic Field

As was discussed in Section 4.1, the magnetic field is determined by monitoring the voltage drop across a  $1\Omega$ , 1%, 5 watt resistor. This resistor, being in series with the solenoid, realizes the same current which is obtained from the voltage record through the relation

$$I = V \left( \frac{1}{R} + \frac{1}{Z} \right). \quad (5.1)$$

$Z$  is the characteristic impedance of the monitoring cable and  $R$  is the  $1\Omega$  resistor. The applied field is in turn obtained from

$$H_e = 0.4\pi NI.$$

These two equations provided the recorded values for the magnetic field. The corrections due to demagnetizing and finite inductance effects were not made.

They were canceling corrections and at best 2% corrections individually. Consideration of errors incurred by measuring R and N along with the associated voltage and calibration records gave an rms error in determining  $H_e$  of  $\pm 2\%$ .

### 5.2. Uniaxial Strain Field

The primary method used to calculate the state of strain in the YIG was through equation of state knowledge of the intermediate materials and measured projectile velocities. The necessary equations of state were presented in Section 4.2.2. The experimental procedure required creation of the same state of strain over a series of shots. The ability to do this relied on the reproducibility of the projectile velocity. It was found that the projectile velocity was constant within 1% over a series of shots. In this analysis, the average projectile velocity was assumed for the entire series.

Calculation of the state of strain in the YIG proceeds as follows. Upon impact of the projectile, the initial state ( $P'$ ,  $u'$ , and  $n'$ ) behind the initial shock in the Lucite is obtained from requirements of continuous  $P'$  and  $u'$  across the projectile-Lucite interface. Simultaneous solution of the projectile  $P - u$  relation and the Lucite  $P - u$  relation (Equation (4.4)) gives  $P'$  and  $u'$ . Equation (4.8) can then be solved for  $n'$ . This is the reference state for the recentered Hugoniot which is used to obtain the state behind the shock reflected from the YIG-Lucite interface. The state of strain in the YIG requires simultaneous solution of the system of equations

$$P = \frac{\left[ \frac{\Gamma_0}{2} P' n + P_H^0(n) \left( 1 - \frac{\Gamma_0}{2} n \right) \right]}{1 - \frac{\Gamma_0}{2} (n - n')} \quad (5.2)$$

$$P = P' + \frac{(u - u')^2}{V_0(n - n')} , \quad (5.3)$$

and

$$P = \rho_0^\gamma Z u \quad (5.4)$$

which relate mechanical parameters when the shock wave, initially in the Lucite, traverses the Lucite-YIG interface. This is a system of three equations in three unknowns;  $P$ ,  $u$ , and  $n$ . The first is Equation (4.7) with the pressure on the Hugoniot recentered about  $P'$  and  $n'$  in the Lucite. The second is obtained from mass and momentum jump conditions across the reflected shock in the Lucite. The third is an elastic  $P - u$  relation for YIG. The system of three equations was solved numerically by a Newton-Raphson iteration technique for the required mechanical parameters.

A technique devised to serve as a consistency check on the numerical methods and equations of state used was to substitute a quartz gauge for the YIG. To be consistent, the actual recorded stress should agree with that calculated through the previous numerical procedure. This was found to be the case within  $\pm 4\%$  over several shots. The variation was not consistently above or below.

Also observed on the quartz gauge records was the deterioration in the stress profile due to propagation through the 1 mil copper-epoxy grid. The effect on the profile was to create a finite rise time of approximately 50 nanoseconds. After the quartz gauge profiles were corrected for finite strain,<sup>53</sup> there still existed a slight ramp of less than 2% across the recording time of the quartz. Although this may be due to incorrect compensation for finite strain, it may also be the effect of dissipation in propagating the stress wave through 1.5 mm of Lucite as has been observed by Barker and

Hollenbach.<sup>57</sup> This possible effect was ignored. It would be slight in any case as can be seen from the profiles published by Barker and Hollenbach.

In summary, the projectile velocity for a series of shots was assumed to be the average obtained from these shots. The state of strain in the YIG was obtained with this projectile velocity and the calculation described in this section. This calculation of the strain should be accurate to  $\pm 5\%$ .

### 5.3. Transverse Magnetization

The last experimental parameter required is the magnetization corresponding to a given magnetic field and shock induced anisotropy field. This is obtained by measuring the reduction in magnetization,  $\delta M$ , assuming that prior to arrival of the shock wave the material is in a state of magnetic saturation. The magnetization is then

$$M = M_s + \delta M$$

where  $M$  is negative.  $\delta M$  is obtained through

$$\delta M = \frac{10^8}{4\pi bND} \epsilon \quad (5.5)$$

as discussed in Section 4.3 where it was assumed that  $\epsilon$  was constant, produced by a steady state shock wave progressing through the magnetic medium.

A typical oscilloscope record from which this magnetic information must be deduced is shown in Figure 5.1. A negative emf is developed during the first transit of the wave corresponding to the expected demagnetization of the magnetic material. The subsequent behavior is determined by alternate remagnetization and demagnetization as the stress wave reverberates back and forth in the magnetic material. A fairly accurate acoustic velocity in YIG can be determined from these records. Only the first half cycle is utilized in analysis of the magnetic state behind the shock.

The analysis in Section 4.3 assumed that a steady state shock existed in the material. Thus, if a square shock enters the medium one would ideally expect the recorded emf to be a square pulse and the analysis would be trivial. This behavior is not the case. Consequently, the factors which complicate this behavior must be addressed.

The first problem is due to the finite rise of the stress profile brought about by its transit through the solenoid face. The expected emf can be shown to be of the form in Figure 5.2(a). This can be seen most easily by considering an incremental application of Equation (4.13). There will be a finite rise to the demagnetization approaching a constant value when the wave is completely in the medium.

The second effect is due to relief waves generated at the lateral limits of the magnetic material. The slabs of YIG used in this work had an aspect ratio of 10 to 1. A first approximation calculation can be made by assuming the relief behavior shown in Figure 5.3. If the longitudinal strain in the unaffected material is  $e$ , then the equivalent strain in an element of the relieved material is

$$e' = \frac{2(\mu + \lambda)}{2\mu + \lambda} e, \quad (5.6)$$

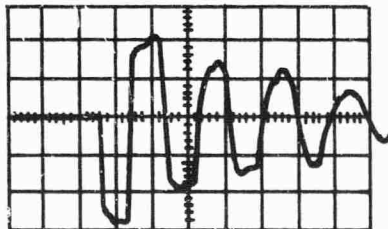


Fig. 5.1.--Oscilloscope record of shot no. 70-039. 0.2  $\mu$ s per division.

obtained from consideration of static displacement in the two dimensional elastic problem.  $\lambda$  and  $\mu$  are the Lamé constants. The emf produced by the demagnetization corresponding to a given state of strain is

$$\mathcal{E} = 4\pi 10^{-8} bND\delta M(e),$$

ignoring the relief problem. By considering this approximation to the relief problem, the induced emf becomes

$$\mathcal{E} = 4\pi 10^{-8} ND((b - 2Dt)\delta M(e) + 2Dt\delta M(e'))$$

or, after reorganizing, the expression becomes

$$\mathcal{E} = 4\pi 10^{-8} bND\delta M(e) \left[ 1 + \left( \frac{\delta M(e')}{\delta M(e)} - 1 \right) \frac{2D}{b} t \right]. \quad (5.7)$$

This equation predicts that the lateral stretching due to relief waves produces a linear increase in emf over that predicted for the infinite slab. The expected behavior is shown in Figure 5.2(b).

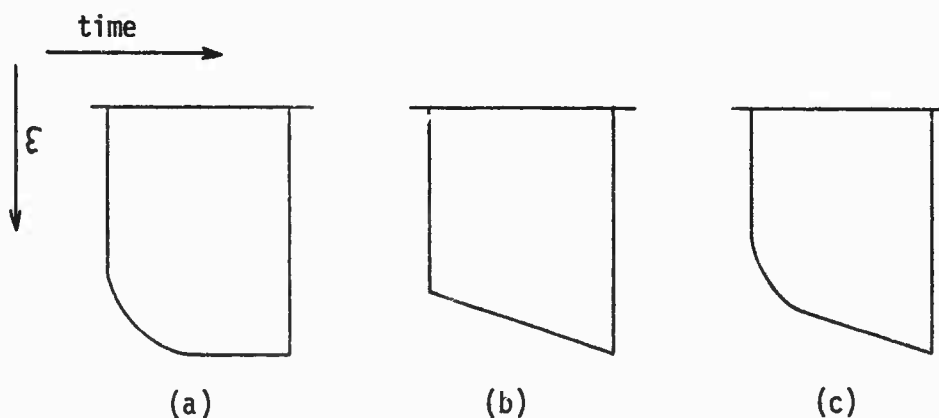


Fig. 5.2.--Effect on the demagnetization profile due to  
(a) finite rise time of strain wave, (b) lateral relief waves,  
and (c) combined effect.

The total behavior due to the superposition of the effects of finite rise and relief waves would be as shown in Figure 5.2(c). This expectation has been supported by the experimental profiles obtained. See Figure 5.5. From these records a consistent means of obtaining the magnetization in the shocked, unrelieved material must be determined. A logical method would be to extrapolate the linear slope in Figure 5.2(c) back to zero time and accept this value of  $\epsilon$  as that required in Equation (5.5). Unfortunately, this is difficult to do consistently. This is especially true for the lower demagnetization shots where the signal to noise ratio was sufficiently low enough to frustrate a quantitative analysis of this kind.

The following is a description of the method used to analyze the experimental demagnetization data. Although less satisfying than that proposed in the last paragraph, this method yields a consistent and conservative description of the measurements. On every record there are distinct and well defined upper and lower bounds to the emf required in Equation (5.5) as shown in Figure 5.4.  $\epsilon_{\min}$  is determined when approximately 70% of the full stress profile initially enters the medium. The 70% is obtained from a reverberation Hugoniot analysis at the solenoid grid.  $\epsilon_{\max}$  incorporates the

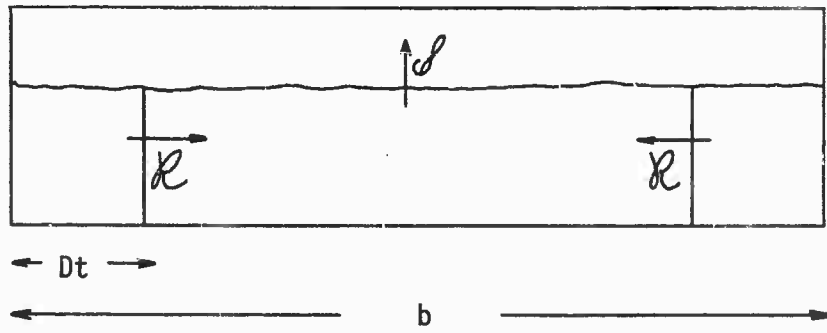


Fig. 5.3.--First approximation geometry of lateral relief wave behavior.

required emf plus the full effect of the lateral relief problem. Thus, one can safely assume that the required emf is

$$\epsilon_{\min} < \epsilon < \epsilon_{\max}$$

The procedure used here was to accept

$$\epsilon = \frac{1}{2} (\epsilon_{\min} + \epsilon_{\max}) \quad (5.8)$$

as the value required in Equation (5.5). The reported value for  $\epsilon$  was this average corrected for the moving pickup coil effect which approached 10% at the lowest demagnetization realized. The difference between  $\epsilon_{\max}$  and  $\epsilon_{\min}$  was accepted as error in the measurement. This was the dominant error.

#### 5.4. Experimental Data

In Table 4, the experimental results of this work are presented in a form consistent with the discussion in the preceding three sections. Figure 5.5 gives the raw oscilloscope profiles resulting from the demagnetization during the first transit of the shock wave. The horizontal coordinate is time

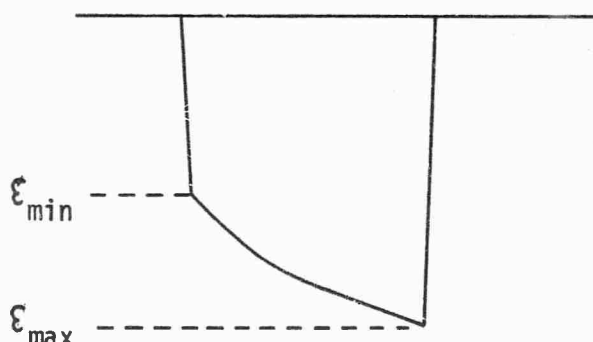


Fig. 5.4.--Emf extremes used in analyzing the demagnetization profile.

in 0.25 microsecond increments. The vertical coordinate is the actual emf developed across the pickup coil. In Figure 5.6, the experimental magnetization curves are presented along with the theoretical curves for the interacting grain and independent grain assumptions. The two series of shots correspond to approximately one-third and two-thirds of the Hugoniot elastic limit in YIG. This has been reported as 64 kbars<sup>10</sup> (attributed to R. A. Graham). In Figure 5.7, the data are plotted as a function of the normalized field  $H_e/e$  against which the predicted magnetization curves for any induced anisotropy field are self similar. The vertical error bars are determined by the experimental extremes as discussed in Section 5.3. The horizontal error bars are  $\pm 6\%$  which is the rms error for  $H_e$  and  $e$ .

TABLE 4.--Experimental results

Shot no.	Projectile velocity (mm/ $\mu$ s)	Projectile material	Mean strain in YIG	Magnetic field (oe)	Induced <sup>a</sup> emf (volts)	Specimen width (cm)	$\delta M/M_s$ <sup>b</sup>
70-016	0.598			359	20.5	1.060	$0.332 \pm .066$
70-030 <sup>c</sup>	0.602			245	-----	1.063	$0.602 \pm .100$
70-039	0.600	Plexiglass ROHM and HASS	-0.0083	258	62.4	1.067	$0.515 \pm .033$
70-053	0.601	Type-G		588	11.2	1.075	$0.089 \pm .034$
70-057	0.596			494	21.6	1.085	$0.173 \pm .037$
70-059	0.598			680	4.6	1.081	$0.039 \pm .015$
71-002	0.597			421	30.3	1.023	$0.260 \pm .055$
71-013	0.598			787	2.5	1.081	$0.018 \pm .010$
71-015	0.551	Aluminum oxide WESGO-995		660	48.5	1.068	$0.400 \pm .030$
71-016	0.555		-0.0162	935	20.5	1.032	$0.173 \pm .038$

<sup>a</sup>This emf was developed across 10 turn pickup coils with the exception of shot no. 70-016 which used a 5 turn pickup coil. The values were obtained through Equation (5.8).

<sup>b</sup>Calculated with an  $M_s$  of 128 gauss. See Section 4.4.

<sup>c</sup>On this shot, the solenoid was prematurely shorted. These values were obtained by estimating the field due to residual current and knowledge of the circuit inductances and resistances.

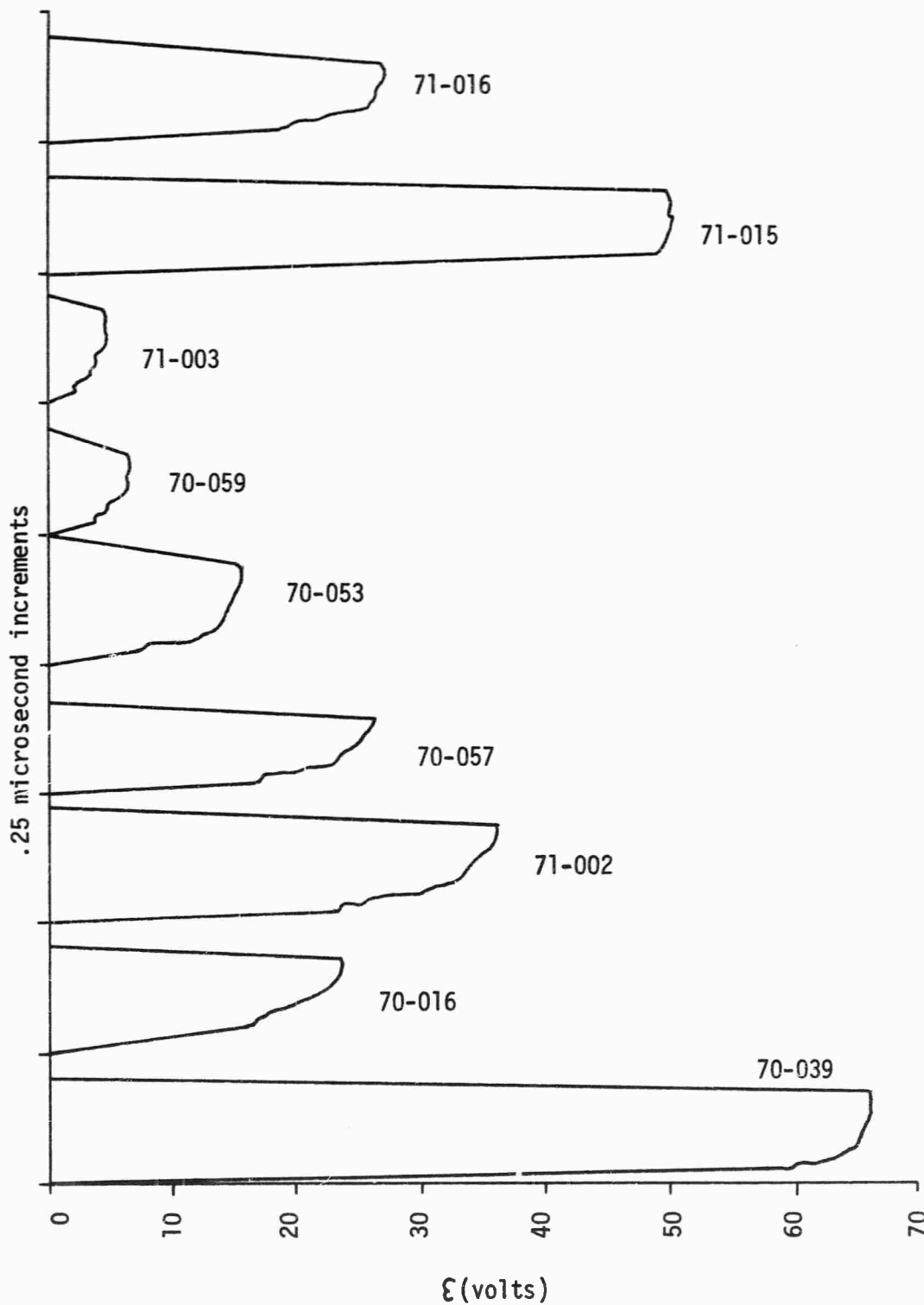


Fig. 5.5.--Oscilloscope profiles of the demagnetization process for the data presented in Table 4.

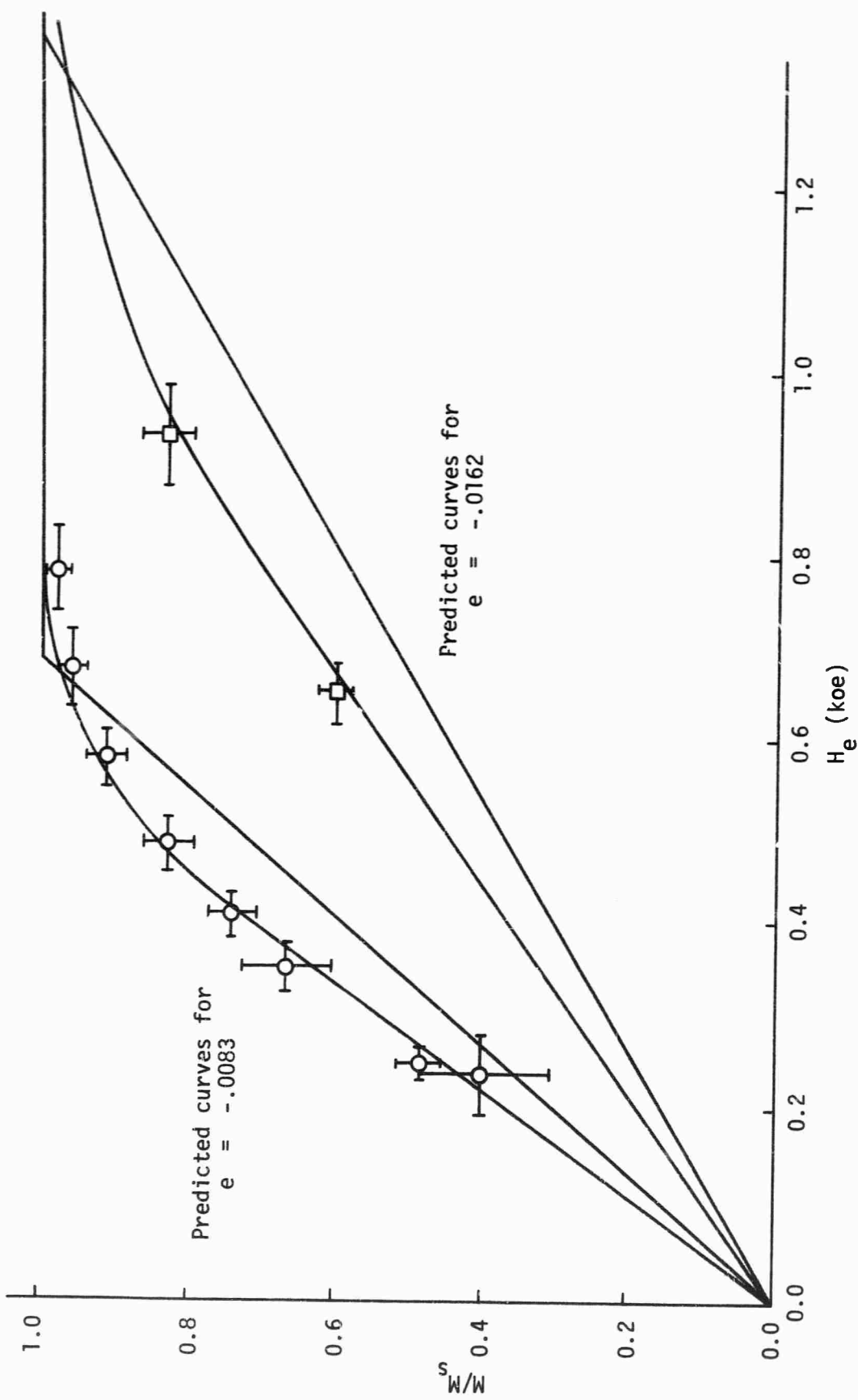


Fig. 5.6.--Experimental data with theoretical magnetization curves for two strain induced anisotropy fields. Circles correspond to strain of  $-.0083$ . Squares correspond to strain of  $-.0162$ . Smooth curves correspond to independent grain theory. Broken curves correspond to interacting grain theory.

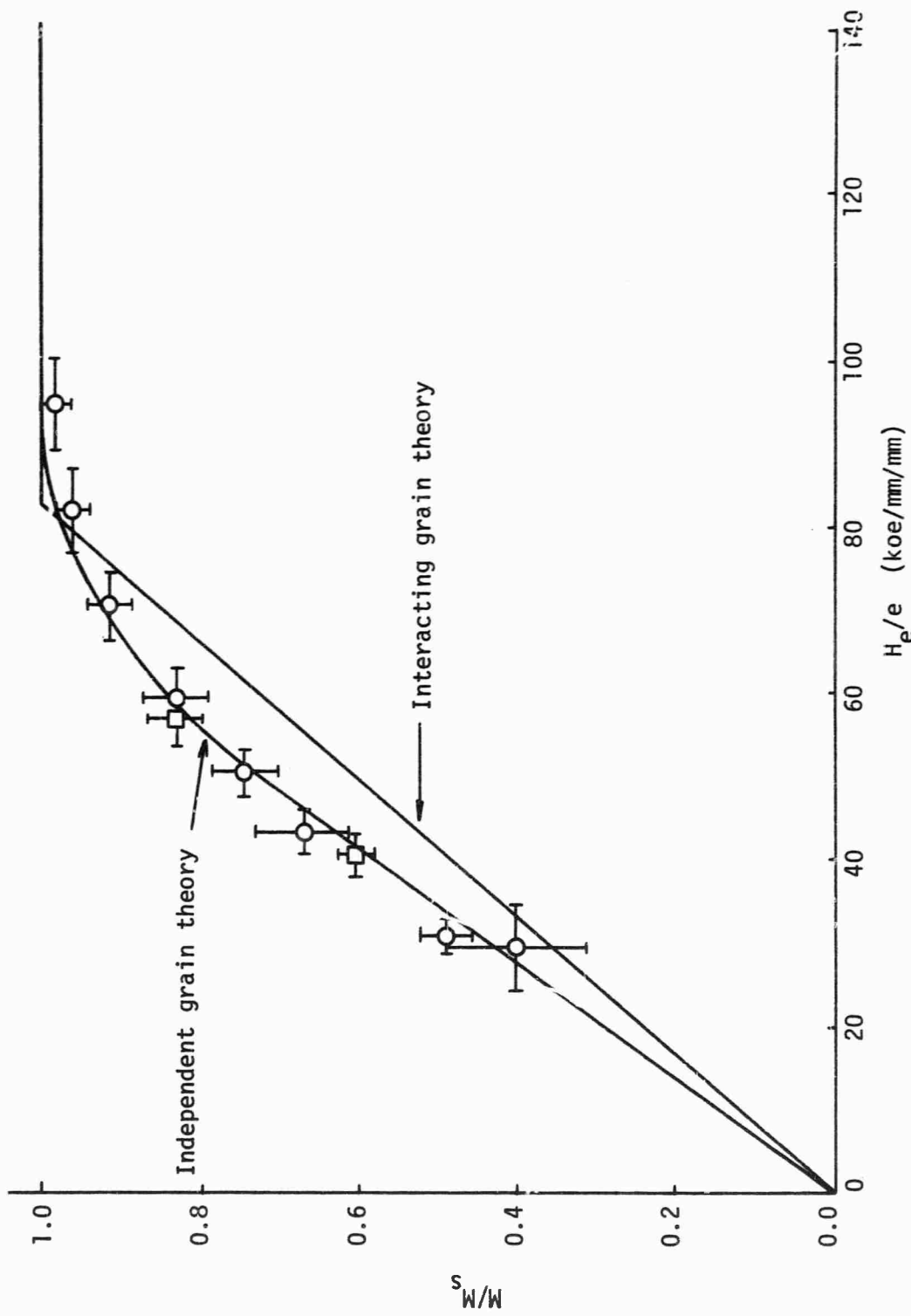


Fig. 5.7.—Data plotted to exhibit theoretically predicted self similarity of magnetization curves against the parameter  $H_e/e$ .

## CHAPTER VI

### DISCUSSION AND CONCLUSIONS

#### 6.1. Discussion

The use of equilibrium thermodynamics to describe the behavior of the shocked ferromagnetic material assumes that equilibrium is reached within a few nanoseconds after passage of the shock wave. Magnetic relaxation times observed by other methods suggest that this very likely occurs. However, the results of the present work lend additional confidence to this assumption.

Within the concepts of domain theory, an analysis of the shock induced anisotropy effect on magnetic single crystals has established the following. The equilibrium exchange and dipolar energy increases as the fourth root of the strain while the magnetoelastic anisotropy energy increases linearly with the strain. This means that the contribution of the exchange and dipolar energy to the magnetic behavior is significant at low strains but becomes negligible in the high elastic and plastic region. It was deduced that domain walls in the direction of strain with normals either perpendicular or parallel to the applied field differed only slightly in wall energy. This small energy difference is probably nullified by local crystal defects. However, domain walls normal to the axis of strain incur high energy due to the magnetic volume poles created. It is logical to conclude that a needle or sliver shaped domain structure oriented in the direction of uniaxial strain nucleates behind the shock wave. The magnetization curves predicted for the <100> and <111> problems are linear and differ substantially. This is a consequence of the magnetoelastic anisotropy of YIG ( $b_1 \neq b_2$ ).

In considering the shock induced anisotropy effect on magnetic polycrystals, a critical analysis of the necessary averaging procedure is required. This analysis is concerned with the magnetic interaction between crystal grains. A definition of extreme assumptions concerning the interaction was made in analogy with the procedure used to determine polycrystalline elastic constants.

From one extreme, the interacting grain theory follows. The physics necessary to make this behavior plausible requires an extra-grain domain structure. This in turn demands sufficient contribution from exchange and dipolar forces to make continuous domains across grain boundaries energetically favorable.

Independent grain theory is the other extreme. This behavior is expected if an intra-grain domain structure occurs. Such domain structure arises when exchange and dipolar forces are insufficient to overcome anisotropy forces.

In the present work, experimental data concerning the shock induced anisotropy effect have been obtained for polycrystalline yttrium iron garnet in the region of large elastic strain. The results, presented in Figure 5.6 and Figure 5.7, support the shock induced anisotropy mechanism as a contribution to shock demagnetization. It is further concluded that the independent grain assumption provides a better description of the magnetic behavior of ferromagnetic material in the shocked state. Also established is the validity of the parameter  $H_e/e$  in characterizing the magnetization curve. This is seen in Figure 5.7 where the experimental magnetization curves, plotted as a function of this parameter, are self similar.

In retrospect, independent grain behavior appears more logical than interacting grain behavior. Domain theory predicts that the equilibrium

exchange and dipolar energy will be negligible compared to the remaining energy terms. It follows that domain walls will be extremely cheap and an inter-grain domain structure will occur. Considering this, one expects independent grain behavior. Conversely, experimental confirmation of the independent grain theory indirectly supports the validity of the domain theoretical calculation which predicts the strain dependence of the equilibrium exchange and dipolar energy.

From the domain theoretical calculation, it was concluded that a sliver or needle shaped domain structure nucleates behind the shock front. This domain structure is an effect rather than a cause since it provides negligible contribution to the shape of the magnetization curve of the shock created ferromagnetic material in the region of large elastic and plastic strain.

It begins to appear that the prediction of magnetic behavior behind the shock front is much simpler than the equivalent prediction in unstrained material. First, the equilibrium exchange and dipolar energy can be ignored in favor of the much simpler induced anisotropy energy. This is definitely not the case in unstrained material. Secondly, in polycrystalline material it appears that the magnetic grain-grain interaction effects are not substantial and magnetic properties can be obtained by simply averaging the behavior of a single independent grain.

From this, one might speculate on the magnetic response of natural or meteoritic material subject to similar shock loading. Here one is confronted with many additional complications. Chemical and compositional gradients along with coexistence of nonmagnetic and magnetic phases produce variations in the saturation magnetization, exchange integral, and magnetoelastic properties. It would be extremely complicated to construct an adequate energy expression to describe this material. However, from the results of the work described

here, one would expect the magnetic response of a local region to depend only on the induced anisotropy in that region and be independent of long range interaction with neighboring material. Consequently, the macroscopic magnetic behavior should be predictable from a similar average over the chemical and compositional structure of the material.

The effect of porosity, as discussed in Section 3.4, is not expected to contribute significantly in the region of the magnetization curve where the experimental data was obtained. The present experimental results confirm this. The porosity effect is expected to become substantial in the lower region of the magnetization curve.

A consistent treatment of the contribution of finite strain to the shock induced anisotropy effect is carried out in Appendix III with the thermodynamics developed in Chapter II. This is required by the high strains considered in this work. Calculations show that the contribution is not substantial. The experimental data verify this conclusion. It follows that, at least for the present material, the conventional magnetoelastic theory of Becker and Doring provides an adequate description of the shock induced anisotropy effect.

The experimental technique developed for this work provides a simple means of measuring the state of magnetization in shocked material. The fundamental difficulties, discussed thoroughly in Section 5.3, are degradation of the shock profile when passing the solenoid grid and lateral rarefaction waves. The first problem can be circumvented by a proper choice of solenoid material at the grid interface as was experimentally established in Section 4.2.1. The second problem could be minimized by better design of the pickup coil-specimen geometry. It is believed that this technique could be useful in more general investigation of the magnetostatic properties of materials.

### 6.2. Summary

The conclusions reached and results obtained during the course of the present work are as follows:

1. Equilibrium thermodynamics provides an adequate description of the shock induced anisotropy effect.
2. Established concepts of domain theory predict that the equilibrium exchange and dipolar energy is proportional to the fourth root of the strain and is negligible in the high elastic and plastic shock region.
3. A needle or sliver shaped domain structure oriented in the direction of shock propagation is expected to nucleate behind the shock front.
4. Consideration of the shock induced anisotropy effect in magnetic polycrystals revealed the importance of magnetic grain-grain interaction. Assumptions of interacting grains and independent grains were defined to describe the possible extremes of this interaction.
5. Data on polycrystalline yttrium iron garnet were obtained in the region of large elastic strain. The results support the independent grain theory as more representative of actual behavior.
6. The experimental results indirectly support the domain theoretical analysis.
7. The effect of porosity has been shown, by analysis and experiment, to be small in the region of the magnetization curve considered.
8. Conventional magnetoelastic theory provides a sufficient characterization of the shock induced anisotropy effect for strains up to at least two-thirds the elastic limit.
9. An experimental technique capable of magnetic measurements on the shocked material has been designed, implemented, and analyzed.

## REFERENCES

1. J. P. Joule, Sturgeons Annals of Electricity 8, 219 (1842).
2. E. Villari, Ann. Phys., Lpz. 126, 87 (1865).
3. R. Becker and W. Döring, Ferromagnetismus (Julius Springer, Berlin, 1939).
4. C. Kittel, Rev. Mod. Phys. 21, 541 (1949).
5. W. F. Brown Jr., Magnetoelastic Interactions (Springer-Verlag Inc., New York, 1966).
6. E. B. Royce, J. Appl. Phys. 37, 4066 (1966).
7. E. B. Royce, "Shock-Induced Demagnetization of Nickel Ferrite, Yttrium Iron Garnet, and Iron," in Behavior of Dense Media under High Dynamic Pressures (Gordon and Breach, New York, 1968), p. 419.
8. J. W. Shaner and E. B. Royce, J. Appl. Phys. 39, 492 (1968).
9. G. E. Seay, R. A. Graham, R. C. Wayne, and L. D. Wright, Bull. Am. Phys. Soc. 12, 1129 (1967).
10. L. C. Bartel, J. Appl. Phys. 40, 661 (1969).
11. L. C. Bartel, J. Appl. Phys. 40, 3988 (1969).
12. R. C. Wayne, G. A. Samara, and R. A. Lefever, J. Appl. Phys. 41, 633 (1970).
13. H. B. Callen, Thermodynamics (John Wiley and Sons, Inc., New York, 1960).
14. J. D. Jackson, Classical Electrodynamics (John Wiley and Sons, Inc., New York, 1962).
15. W. Band, Introduction to Mathematical Physics (D. Van Nostrand Company, Inc., New Jersey, 1959).
16. H. A. Leupold, Am. J. Phys. 37, 1047 (1969).
17. W. F. Brown Jr., Magnetostatic Principles in Ferromagnetism (North-Holland Publ. Co., Amsterdam, 1962).
18. D. C. Mattis, The Theory of Magnetism (Harper and Row, New York, 1965).

19. K. W. H. Stevens, "Spin Hamiltonians," in Magnetism, G. T. Rado and H. Suhl, Eds. (Academic Press, New York, 1963), Vol. I.
20. J. S. Smart, Effective Field Theories of Magnetism (W. B. Saunders Company, Philadelphia, 1966).
21. K. J. Yosida, J. Appl. Phys. 39, 511 (1968).
22. A. H. Morrish, The Physical Principles of Magnetism (John Wiley and Sons, Inc., New York, 1965).
23. D. Bloch, F. Chaissé, and R. Panthenet, J. Appl. Phys. 37, 1401 (1966).
24. P. W. Anderson, "Exchange in Insulators: Superexchange, Direct Exchange, and Double Exchange," in Magnetism, G. T. Rado and H. Suhl, Eds. (Academic Press, New York, 1963), Vol. I.
25. F. Bitter, Selected Papers and Commentaries (The M.I.T. Press, Massachusetts Institute of Technology, 1968).
26. J. Kanamuri, "Anisotropy and Magnetostriction of Ferromagnetic and Anti-ferromagnetic Materials," in Magnetism, G. T. Rado and H. Suhl, Eds. (Academic Press, New York, 1963), Vol. I.
27. R. N. Thurston, "Wave Propagation in Fluids and Normal Solids," in Physical Acoustics, W. P. Mason, Ed. (Academic Press, New York, 1964), Vol. IA.
28. R. Toupin, J. Rational Mechanics and Analysis 5, 850 (1956).
29. A. L. Cauchy, Oeuvres, Ser. I 2, 356 (1850).
30. D. E. Eastman, Phys. Rev. 148, 530 (1966).
31. W. F. Brown Jr., Micromagnetics (John Wiley and Sons (Interscience), New York, 1963).
32. C. Kittel and J. K. Galt, "Ferromagnetic Domain Theory," in Solid State Physics, F. Seitz and D. Turnbull, Eds. (Academic Press, New York, 1957), Vol. III.
33. L. Landau and E. Lifshitz, Physik. Z. Sowjetunion 8, 153 (1935).
34. K. S. Aleksandrov and L. A. Aizenberg, Sov. Phys.-Dokl. 11, 323 (1966).
35. O. L. Anderson, "Determination and Some Uses of Isotropic Elastic Constants of Polycrystalline Aggregates Using Single-Crystal Data," in Physical Acoustics, W. P. Mason, Ed. (Academic Press, New York, 1965), Vol. IIIB.
36. W. Voigt, Lehrbuch der Kristallphysik (Teubner, Leipzig, 1928).
37. A. Reuss, Z. Angew. Math. Mech. 9, 49 (1929).

38. N. S. Akulov, Z. Physik 66, 533 (1930).
39. K. V. Vladimirska, Compt. Rend. (Doklady) Acad. Sci. URSS 41, 10 (1943).
40. E. W. Lee, Rep. Progr. Phys. 18, 184 (1955).
41. H. B. Callen and N. Goldberg, J. Appl. Phys. 36, 976 (1956).
42. J. E. Knowles, Brit. J. Appl. Phys. 1, 987 (1968).
43. R. Wadas, Electron Technology, Warsaw 2, 63 (1969).
44. R. Carey and E. D. Isaac, Magnetic Domains and Techniques for Their Observation (Academic Press, New York, 1966).
45. R. R. Birss, Proc. Phys. Soc. 75, 8 (1960).
46. E. W. Lee, Proc. Phys. Soc. 72, 249 (1959).
47. S. Shtrikman and D. Treves, "Micromagnetics," in Magnetism, G. T. Rado and H. Suhl, Eds. (Academic Press, New York, 1963), Vol. III.
48. D. E. Grady, Bull. Amer. Phys. Soc. 15, 1603 (1970).
49. J. Smit and H. P. J. Wijn, Ferrites (John Wiley and Sons, Inc., New York, 1959), p. 119.
50. The Wilkenson Company, P. O. Box 1307, Westlake Village, Calif. 91360.
51. G. R. Fowles, G. E. Duvall, J. Asay, P. Bellamy, F. Feistmann, D. Grady, T. Michaels, and R. Mitchell, Rev. Sci. Instrum. 41, 984 (1970).
52. V. N. Mineev and E. V. Savinov, Sov. Phys. JETP 25, 411 (1967).
53. R. A. Graham, F. W. Neilson, and W. B. Benedick, J. Appl. Phys. 36, 1775 (1965).
54. Western Gold and Platinum Company, 525 Harbor Blvd., Belmont, Calif.
55. T. J. Ahrens, W. H. Gust, and E. B. Royce, J. Appl. Phys. 39, 4610 (1968).
56. T. P. Liddiard Jr., Fourth Symposium on Detonation, USNOL, 1965).
57. L. M. Barker and B. E. Hollenbach, J. Appl. Phys. 41, 4208 (1970).
58. G. E. Duvall and G. R. Fowles, "Shock Waves," in High Pressure Physics and Chemistry, R. S. Bradley, Ed. (Academic Press, New York, 1963), Vol. II.
59. J. R. Asay, D. L. Lamberson, and A. H. Guenther, J. Appl. Phys. 40, 1768 (1969).
60. R. E. Barker Jr., J. Appl. Phys. 38, 4234 (1967).

61. M. H. Rice, R. G. McQueen, and J. M. Walsh, "Compression of Solids by Strong Shock Waves," in Solid State Physics, F. Seitz and D. Turnbull, Eds. (Academic Press, New York, 1958), Vol. VI.
62. Semi-Elements Inc., Saxonburg, Penn.
63. R. M. Bozorth, Ferromagnetism (D. Van Nostrand Company, Inc., New York, 1951).
64. R. Hill, Proc. Phys. Soc., A 65, 349 (1952).

## APPENDIX I

### TABLE OF THERMODYNAMIC AND ENERGY EXPRESSIONS

TABLE 5.--Thermodynamic and energy expressions

Expression	Note
Total magnetic work	
$\delta W = \frac{1}{4\pi} \int \vec{H} \cdot \vec{\delta B} dV$ $\delta W = \int \vec{H} \cdot \vec{\delta M} dV + \delta \int \frac{H_d^2}{8\pi} dV +$ $\delta \int \frac{H_e^2}{8\pi} dV$	Follows directly from Maxwell's equations.  First term is stored as local energy or dissipated in irreversible processes. Second term is stored as self energy. Also called demagnetizing or dipolar energy. Third term is stored as energy in the external field.
Magnetic work on material only	
$\delta W = \int \vec{H} \cdot \vec{\delta M} dV + \delta \int \frac{H_d^2}{8\pi} dV$ $\delta W = \int \vec{H} \cdot \vec{\delta M} dV - \frac{1}{2} \delta \int \vec{M} \cdot \vec{H}_d dV$ $\delta W = \int \vec{H}_e \cdot \vec{\delta M} dV$	Work on external field is not considered.  The second term is an alternative form for self energy.  Follows from magnetostatic theorems (p. 8) or directly from Faraday's law.

TABLE 5--Continued

Expression	Note
Energy	
$\delta U \leq T\delta S + \int \vec{H}_e \cdot \vec{\delta M} dV$	Combined first and second law of thermodynamics.
$\delta E \leq T\delta S - \int \vec{M} \cdot \vec{\delta H}_e dV$	$S$ and $\vec{H}_e$ are independent variables for this energy expression.
$E = U - \int \vec{H}_e \cdot \vec{M} dV = U + \int \vec{\epsilon}_H dV$	Legendre transformed energy expression. Second term in either expression is interaction energy in external field.
$E = \int \vec{\epsilon}_H dV + \int \vec{\epsilon}_d dV + \int \vec{\epsilon}_{LOC} dV$	Internal energy separates into local energy and long range self energy.
$E = \int \vec{\epsilon}_H dV + \int \vec{\epsilon}_d dV + \int \vec{\epsilon}_{ex} dV + \int \vec{\epsilon}_A dV$	Local energy separates into exchange energy and anisotropy energy.
$E = \int \vec{\epsilon}_H dV + \int \vec{\epsilon}_d dV + \int \vec{\epsilon}_{ex} dV + \int \vec{\epsilon}_K dV + \int \vec{\epsilon}_{me} dV$	Anisotropy energy separates into crystalline energy and magnetoelastic energy.

## APPENDIX II

### LIST OF SYMBOLS

#### Chapters II and III

- $\vec{H}$  = magnetic field intensity =  $\vec{H}_e + \vec{H}_d$   
 $\vec{H}_e$  = external field  
 $\vec{H}_d$  = demagnetizing field  
 $\vec{M}$  = magnetization = magnetic moment/volume  
 $\vec{M}_s$  = saturation magnetization =  $M_s \vec{\alpha}$   
 $\vec{\alpha}$  =  $(\alpha_1, \alpha_2, \alpha_3)$  = direction cosines of magnetization  
referred to crystal axes  
 $S$  = entropy  
 $T$  = temperature  
 $U$  = total energy  
 $E$  = total Legendre transformed energy  
 $\epsilon$  = specific energy corresponding to  $E$   
 $\epsilon_H$  = interaction energy  
 $\epsilon_d$  = demagnetization energy  
 $\epsilon_{ex}$  = exchange energy  
 $\epsilon_K$  = crystal anisotropy energy  
 $\epsilon_{me}$  = magnetoelastic energy  
 $\epsilon_A$  = total anisotropy energy =  $\epsilon_K + \epsilon_{me}$   
 $\epsilon_{LOC}$  = local energy =  $\epsilon_K + \epsilon_{me} + \epsilon_{ex}$   
 $x_i$  = Eulerian coordinates

- $a_i$  = Lagrangian coordinates  
 $\partial x_i / \partial a_j$  = deformation gradients  
 $E_{ij}$  = finite strain  
 $e_{ij}$  = infinitesimal strain  
 $e$  = extension =  $\rho_0 / \rho - 1$   
 $\rho$  = density  
 $\mathcal{S}$  = symbol for shock wave  
 $\mathcal{R}$  = symbol for rarefaction wave  
 $K_1$  = crystal anisotropy constant  
 $b_1, b_2$  = first order magnetoelastic constants  
 $B$  = average of first order magnetoelastic constants  
 $B_{111}$ , etc. = second order magnetoelastic constants  
 $\sigma_w$  = domain wall energy/area  
 $D$  = domain width  
 $L$  = ferromagnetic slab thickness  
 $A$  = exchange constant  
 $F(\Omega)$  = distribution function of magnetization vectors  
 $n_1, n_2$  =  $-M_s / 2b_1 e, -M_s / 2b_2 e$   
 $\sigma_x, \sigma_y$  = stress components  
 $P$  = hydrostatic pressure  
 $\bar{P}$  = mean pressure  
 $\mu$  = shear modulus

#### Chapters IV and V

- $I$  = current  
 $\epsilon_0$  = initial voltage on capacitor  
 $C$  = capacitance  
 $L$  = inductance

- N = solenoid turns/cm or number of turns in pickup coil  
 $\vec{A}$  = magnetic vector potential  
D = shock or longitudinal velocity or demagnetizing factor  
V = specific volume or oscilloscope voltage  
Z = mechanical impedance =  $\rho_0 D$  or transmission line impedance  
P = longitudinal stress  
u = particle velocity  
E = energy  
S = entropy  
 $\Gamma$  = Grüneisen constant  
 $P_H^0(V)$  = initial Hugoniot  
 $\eta = 1 - V/V_0$   
 $P'$ ,  $V'$ ,  $E'$ ,  $\eta'$  = thermodynamic state on initial Hugoniot  
 $\epsilon(t)$  = emf developed across pickup coils  
b = width of pickup coil  
 $\Phi$  = magnetic flux  
 $\delta M$  = shock induced change in magnetization  
 $\epsilon'$  = shock induced emf across solenoid  
 $\epsilon''$  = emf due to magnetic velocity gauge effect  
 $\epsilon_{\max}, \epsilon_{\min}$  = defined by maximum and minimum in demagnetization profile

## APPENDIX III

### FINITE STRAIN EFFECT

The work in Chapters III, IV, and V assumed the conventional magneto-elastic theory of Becker and Doring. It has been shown by Brown<sup>5</sup> that this theory, which assumes infinitesimal strain from the start, is inconsistent in small orders of strain. This inconsistency is normally of no consequence in magnetostriuctive processes due to the extremely small strains involved (the order of  $10^{-5}$ ). In the present effect, strains of  $10^{-2}$  or larger are realized. For this reason, it is necessary that the effect of finite strain be considered.

#### III.1. The Finite Strain Tensor

In the spirit of Thurston,<sup>27</sup> the deformation gradient for uniaxial strain colinear with the unit vector  $\hat{n}$  is

$$\frac{\partial x_i}{\partial a_j} = e n_i n_j + \delta_{ij} \quad (\text{III.1})$$

where

$$e = \frac{\rho_0}{\rho} - 1$$

is the extension in the direction of uniaxial strain, the  $x_i$  are the Eulerian or spacial coordinates, and the  $a_j$  are the Lagrangian or material coordinates. From the Lagrangian definition of finite strain,

$$E_{ij} = \frac{1}{2} \left( \frac{\partial x_k}{\partial a_i} \frac{\partial x_k}{\partial a_j} - \delta_{ij} \right),$$

one obtains the finite uniaxial strain tensor

$$E_{ij} = \left( e + \frac{e^2}{2} \right) n_i n_j. \quad (\text{III.2})$$

### III.2. Finite Strain Correction to Interacting Grain Theory

It was shown in Section 3.2 that crystal anisotropy energy does not contribute in the first order to the shock induced anisotropy effect under conventional magnetoelastic theory. This does not follow from finite strain theory. From Equation (2.13),

$$\epsilon_K = K_1 (\alpha_1^{*2} \alpha_2^{*2} + \alpha_2^{*2} \alpha_3^{*2} + \alpha_3^{*2} \alpha_1^{*2}), \quad (\text{III.3})$$

where

$$\begin{aligned} \alpha_i^* &= \frac{\partial x_j}{\partial a_i} \alpha_j \\ &= (en_i n_j + \delta_{ij}) \alpha_j. \end{aligned} \quad (\text{III.4})$$

Substituting into Equation (III.3) gives terms, to first order in  $e$ , of the form

$$\begin{aligned} \alpha_1^{*2} \alpha_2^{*2} &= \alpha_1^2 \alpha_2^2 + 2e \alpha_1^2 \alpha_2 (n_2^2 \alpha_2 + n_2 n_3 \alpha_3 + n_2 n_1 \alpha_1) + \\ &\quad 2e \alpha_1^2 \alpha_2^2 (n_1^2 \alpha_1 + n_1 n_2 \alpha_2 + n_1 n_3 \alpha_3) + o(e^2) + \dots \end{aligned}$$

The other terms follow by permuting indices. Collecting terms, using

$$\alpha_1^2 + \alpha_2^2 + \alpha_3^2 = 1,$$

and then averaging with Table 1 gives

$$\varepsilon_K = \frac{K_1}{5} + \frac{2}{5} K_1 e \cos^2 \theta.$$

Since  $K_1$  is usually two to three times smaller than the magnetoelastic constants, this contribution to the shock induced anisotropy effect can be ignored.

In obtaining the magnetoelastic energy correct to second order in the extension, both the first and second order magnetoelastic expressions in Equation (2.13) must be considered. This point has the same origin as the inconsistency first noticed by Brown. The second order correction to the first order magnetoelastic energy will be considered first. This energy expression is

$$\begin{aligned} \varepsilon_{me}^{(1)} = & b_1(E_{11}\alpha_1^{*2} + E_{22}\alpha_2^{*2} + E_{33}\alpha_3^{*2}) + \\ & 2b_2(E_{12}\alpha_1^{*}\alpha_2^{*} + E_{23}\alpha_2^{*}\alpha_3^{*} + E_{31}\alpha_3^{*}\alpha_1^{*}). \end{aligned}$$

With Equation (III.2) and Equation (III.4), this becomes

$$\begin{aligned} \varepsilon_{me}^{(1)} = & b_1 \left[ \left( e + \frac{e^2}{2} \right) (n_1^2 \alpha_1^2 + n_2^2 \alpha_2^2 + n_3^2 \alpha_3^2) + 2e^2 (n_1^4 \alpha_1^2 + n_2^4 \alpha_2^2 + n_3^4 \alpha_3^2) \right. \\ & + 2e^2 (n_1 n_2 \alpha_1 \alpha_2 + n_2 n_3 \alpha_2 \alpha_3 + n_3 n_1 \alpha_3 \alpha_1) \\ & - 2e^2 (n_1^2 n_2 n_3 \alpha_2 \alpha_3 + n_2^2 n_3 n_1 \alpha_3 \alpha_1 + n_3^2 n_1 n_2 \alpha_1 \alpha_2) \Big] \\ & + 2b_2 \left[ \left( e + \frac{e^2}{2} \right) (n_1 n_2 \alpha_1 \alpha_2 + n_2 n_3 \alpha_2 \alpha_3 + n_3 n_1 \alpha_3 \alpha_1) \right. \\ & \left. + e^2 (n_1 n_2 \alpha_1 \alpha_2 + n_2 n_3 \alpha_2 \alpha_3 + n_3 n_1 \alpha_3 \alpha_1) \right] \end{aligned}$$

$$\begin{aligned}
 & + e^2(n_1^2 n_2 n_3 \alpha_2 \alpha_3 + n_2^2 n_3 n_1 \alpha_3 \alpha_1 + n_3^2 n_1 n_2 \alpha_1 \alpha_2) \\
 & + e^2(n_1^2 \alpha_1^2 + n_2^2 \alpha_2^2 + n_3^2 \alpha_3^2) - e^2(n_1^4 \alpha_1^2 + n_2^4 \alpha_2^2 + n_3^4 \alpha_3^2) \\
 & + o(e^3) + \dots
 \end{aligned}$$

Averaging this expression with the aid of Table 1 gives

$$\epsilon_{me}^{(1)} = \left[ \left( \frac{2}{5} b_1 + \frac{3}{5} b_2 \right) e + \left( \frac{14}{10} b_1 + \frac{11}{10} b_2 \right) e^2 \right] \cos^2 \theta$$

for the first order magnetoelastic energy correct to second order in  $e$ .

Note that in the case of isotropy

$$\epsilon_{me}^{(1)} = b \left( e + \frac{5}{2} e^2 \right) \cos^2 \theta.$$

The second order magnetoelastic energy is

$$\begin{aligned}
 \epsilon_{me}^{(2)} = & \frac{1}{2} B_{111} (E_{11\alpha_1^*}^2 + E_{22\alpha_2^*}^2 + E_{33\alpha_3^*}^2) \\
 & + B_{123} (E_{11} E_{22\alpha_3^*}^2 + E_{22} E_{33\alpha_1^*}^2 + E_{33} E_{11\alpha_2^*}^2) \\
 & + 2B_{144} (E_{11} E_{23\alpha_2^*\alpha_3^*} + E_{22} E_{31\alpha_3^*\alpha_1^*} + E_{33} E_{12\alpha_1^*\alpha_2^*}) \\
 & + 2B_{441} (E_{23\alpha_1^*}^2 + E_{31\alpha_2^*}^2 + E_{12\alpha_3^*}^2) \\
 & + 2B_{155} ((E_{11} + E_{22}) E_{12\alpha_1^*\alpha_2^*} + (E_{22} + E_{33}) E_{23\alpha_2^*\alpha_3^*} + \\
 & (E_{33} + E_{11}) E_{31\alpha_3^*\alpha_1^*}) + 4B_{456} (E_{23} E_{31\alpha_1^*\alpha_2^*} + E_{31} E_{12\alpha_3^*\alpha_2^*} \\
 & + E_{12} E_{23\alpha_1^*\alpha_3^*}).
 \end{aligned}$$

In this expression, it is correct to second order in  $e$  to replace  $E_{ij}$  by  $e_{ij}$  and  $\alpha_j^*$  by  $\alpha_j$ . This gives

$$\begin{aligned}
 \epsilon_{me}^{(2)} = & \frac{1}{2} B_{111} e^2 (n_1^4 \alpha_1^2 + n_2^4 \alpha_2^2 + n_3^4 \alpha_3^2) \\
 & + B_{123} e^2 (n_1^2 n_2^2 \alpha_3^2 + n_2^2 n_3^2 \alpha_1^2 + n_3^2 n_1^2 \alpha_2^2) \\
 & + 2B_{144} e^2 (n_1^2 n_2 n_3 \alpha_2 \alpha_3 + n_2^2 n_3 n_1 \alpha_3 \alpha_1 + n_3^2 n_1 n_2 \alpha_1 \alpha_2) + \\
 & 2B_{441} e^2 (n_2^2 n_3^2 \alpha_1^2 + n_3^2 n_1^2 \alpha_2^2 + n_1^2 n_2^2 \alpha_3^2) \\
 & + 2B_{155} e^2 ((n_1^2 + n_2^2) n_1 n_2 \alpha_1 \alpha_2 + (n_2^2 + n_3^2) n_2 n_3 \alpha_2 \alpha_3 \\
 & + (n_3^2 + n_1^2) n_3 n_1 \alpha_3 \alpha_1) \\
 & + 4B_{456} e^2 (n_3^2 n_1 n_2 \alpha_1 \alpha_2 + n_1^2 n_2 n_3 \alpha_2 \alpha_3 + n_2^2 n_3 n_1 \alpha_3 \alpha_1) \\
 & + o(e^3) + \dots
 \end{aligned}$$

Averaging this expression with the aid of Table 1 and neglecting a function of strain only gives the second order magnetoelastic energy correct to second order in  $e$ .

$$\epsilon_{me}^{(2)} = \frac{1}{35} (6B_{111} - 2B_{123} + 3B_{144} + 18B_{155} - 4B_{441} + 6B_{456}) e^2 \cos^2 \theta$$

The total average magnetoelastic energy consistent with the interacting grain theory correct to second order in  $e$  is

$$\begin{aligned}
 \epsilon_{me} = & \left[ \left( \frac{2}{5} b_1 + \frac{3}{5} b_2 \right) e + \left( \frac{14}{10} b_1 + \frac{11}{10} b_2 + \frac{6}{35} B_{111} - \frac{2}{35} B_{123} + \frac{3}{35} B_{144} \right. \right. \\
 & \left. \left. + \frac{18}{35} B_{155} - \frac{4}{35} B_{441} + \frac{6}{35} B_{456} \right) e^2 \right] \cos^2 \theta. \quad (\text{III.5})
 \end{aligned}$$

### III.3. Finite Strain Correction to Independent Grain Theory

The independent grain theory requires solutions of the  $<100>$  problem and the  $<111>$  problem from finite strain theory. For uniaxial strain

along a <100> direction, the magnetoelastic energy reduces to

$$\epsilon_{me}^{<100>} = b_1 E_{11} \alpha_1^{*2} + \frac{1}{2} B_{111} E_{11}^2 \alpha_1^{*2}.$$

Using

$$E_{11} = e + \frac{e^2}{2} \quad (\text{III.6})$$

and

$$\alpha_1^{*2} = (1 + 2e) \alpha_1^2 + o(e^2) + \dots, \quad (\text{III.7})$$

one obtains

$$\epsilon_{me}^{<100>} = \left[ b_1 e + \left( \frac{5}{2} b_1 + \frac{B_{111}}{2} \right) e^2 \right] \alpha_1^2 \quad (\text{III.8})$$

correct to second order in  $e$ .

The solution of the <111> problem is somewhat more difficult. One method is to rotate the first and second order magnetoelastic tensors (fourth and sixth rank tensors, respectively) to a coordinate system coincident with the <111> crystal axes. In this system,

$$\begin{aligned} \epsilon_{me}^{<111>} = & b_{11}' E_{11} \alpha_1^{*2} + b_{12}' E_{11} (\alpha_2^{*2} + \alpha_3^{*2}) + \frac{1}{2} B_{111}' E_{11}^2 \alpha_1^{*2} + \\ & \frac{1}{2} B_{112}' E_{11}^2 (\alpha_2^{*2} + \alpha_3^{*2}) \end{aligned}$$

where

$$b_{11}' = \frac{1}{3} b_1 + \frac{2}{3} b_2,$$

$$b_{12}' = \frac{1}{3} b_1 - \frac{1}{3} b_2,$$

$$B'_{111} = \frac{1}{9} B_{111} + \frac{2}{9} B_{123} + \frac{4}{9} B_{144} + \frac{8}{9} B_{155} + \frac{4}{9} B_{441} + \frac{8}{9} B_{456},$$

and

$$B'_{112} = \frac{1}{9} B_{111} + \frac{2}{9} B_{123} + \frac{1}{9} B_{144} + \frac{2}{9} B_{155} - \frac{2}{9} B_{441} - \frac{4}{9} B_{456}$$

are obtained from the tensor transformation. Using Equation (III.6), Equation (III.7), and

$$\alpha_1^2 + \alpha_2^2 + \alpha_3^2 = 1,$$

one obtains the energy expression

$$\epsilon_{me}^{<111>} = \left[ b_2 e + \left( \frac{5}{2} b_2 + \frac{1}{5} B_{144} + \frac{1}{3} B_{155} + \frac{1}{3} B_{441} + \frac{2}{3} B_{456} \right) e^2 \right] \alpha_1^2. \quad (III.9)$$

With Equation (III.8) and Equation (III.9), one obtains the expressions for  $\eta_1$  and  $\eta_2$  in Equation (3.14) and hence the independent grain magnetization curve. The finite strain correction in either theory was not found to be substantial.

## APPENDIX IV

### MAGNETOELASTIC ENERGY ABOUT A SPHERICAL PORE

In this appendix, the magnetoelastic energy density about a spherical pore in an isotropic elastic magnetic medium subject to hydrostatic pressure will be derived. Figure IV.1 should be referred to for symbols.

It is first necessary to find the strain field about a pore subject to a limiting boundary condition of hydrostatic strain. This is accomplished by finding the displacement field. The displacement field, because of symmetry, is of the form

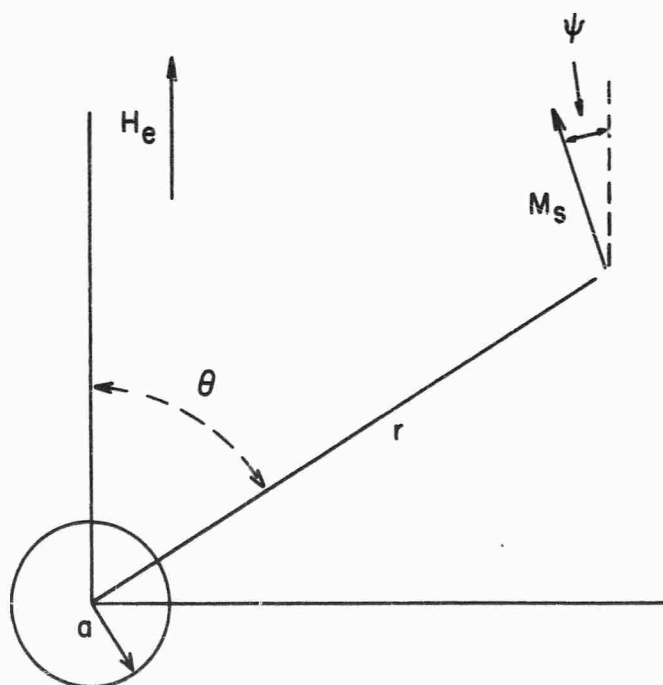


Fig. IV.1.--Spherical cavity of radius  
a.  $M_s \cos\psi$  is the magnetization in the direction of the applied field at the spherical coordinate  $(r, \theta, \phi)$ . There is azimuthal symmetry.

$$\vec{u} = u_r(r) \hat{i}_r.$$

The radial displacement must satisfy Laplace's equation. In spherical coordinates, this becomes

$$\frac{d}{dr} \left[ r^2 \left( \frac{du_r}{dr} \right) \right] - 2u_r = 0.$$

This has the solution

$$u_r = Ar + \frac{B}{r^2}.$$

The limiting boundary condition ( $r \rightarrow \infty$ ) is that the strain be hydrostatic.

$$\left. \frac{du_r}{dr} \right|_{r=\infty} = \left. e_{rr} \right|_{r=\infty} = -\frac{K_T P}{3},$$

where  $K_T$  is the isothermal compressibility. The boundary condition at  $r = a$  is that the normal stress be zero.

$$\sigma_{rr} = \frac{E}{(1+\nu)(1-2\nu)} ((1-\nu)e_{rr} + \nu(e_{\theta\theta} + e_{\phi\phi})) = 0$$

where  $E$  is Young's modulus and  $\nu$  is Poisson's ratio. This boundary condition becomes

$$\left. \frac{du_r}{dr} \right|_{r=a} = \left. e_{rr} \right|_{r=a} = \frac{\nu}{(1-2\nu)} K_T P.$$

The radial displacement field satisfying the boundary conditions is

$$v_r = -\frac{K_T P}{3} r - \frac{P}{4\mu} \frac{a^3}{r^2}$$

where  $\mu$  is the shear modulus. The strain components, obtained from the appropriate derivatives of the displacement field, are

$$e_{rr} = -\frac{K_T P}{3} + \frac{P}{2\mu} \frac{a^3}{r^3},$$

$$e_{\theta\theta} = -\frac{K_T P}{3} - \frac{P}{4\mu} \frac{a^3}{r^3},$$

and

$$e_{\phi\phi} = -\frac{K_T P}{3} - \frac{P}{4\mu} \frac{a^3}{r^3}.$$

The deviatoric strain,  $e_{ij}^d$ , is obtained by subtracting the hydrostatic strain. This is the only part that contributes to the magnetoelastic energy. In local Cartesian coordinates, the deviatoric strain tensor is

$$e_{ij}^d = \frac{P}{4\mu} \frac{a^3}{r^3} \left[ 3 \frac{x_i x_j}{r^2} - \delta_{ij} \right].$$

Using this expression for the strain in the magnetoelastic energy,

$$\begin{aligned} \epsilon_{me} = & b_1(\alpha_1^2 e_{11} + \alpha_2^2 e_{22} + \alpha_3^2 e_{33}) + 2b_2(\alpha_1 \alpha_2 e_{12} + \\ & \alpha_2 \alpha_3 e_{23} + \alpha_3 \alpha_1 e_{31}), \end{aligned}$$

and using the average values in Table 1 where

$$\frac{x_i x_j}{r^2} = n_i n_j,$$

one obtains

$$\epsilon_{me} = \frac{3p}{4\mu} B \frac{a^3}{r^3} \cos^2(\psi + \theta)$$

where

$$B = \frac{2}{5} b_1 + \frac{3}{5} b_2.$$

This is the magnetoelastic energy in Equation (3.16).

## APPENDIX V

### DEVIATION FROM UNIFORM STRAIN

In Chapter III, the assumption was made that a polycrystalline material subject to macroscopic uniaxial strain realizes microscopic uniform strain, where macroscopic and microscopic are relative to the grain size. This is not strictly true. In individual crystallites deviation from uniform strain can be expected. The purpose of this appendix is to obtain a measure of this deviation from uniform strain in cubic polycrystalline material.

If a polycrystalline material is subject to macroscopic uniaxial strain and further constrained to uniform strain in each crystallite, then the associated elastic energy is

$$E_V = \frac{1}{2} m_V e^2$$

where

$$m_V = K_V + \frac{4}{3} \mu_V \quad (V.1)$$

is the longitudinal modulus obtained from the Voigt assumption.<sup>36</sup>

$$K_V = \frac{1}{3} (c_{11} + 2c_{12}) \quad (V.2)$$

and

$$\mu_V = \frac{1}{5} ((c_{11} - c_{12}) + 3c_{44}) \quad (V.3)$$

are the bulk modulus and shear modulus in terms of the elastic stiffness coefficients.

If a polycrystalline material is subject to macroscopic uniaxial strain but constrained locally to uniform stress, then the elastic energy is

$$E_R = \frac{1}{2} m_R e^2$$

where

$$m_R = K_R + \frac{4}{3} \mu_R \quad (V.4)$$

is the longitudinal modulus obtained from the Ruess assumption.<sup>37</sup>

$$K_R = \frac{1}{3} (c_{11} + 2c_{12}) \quad (V.5)$$

and

$$\mu_R = \frac{5}{4(S_{11} - S_{12}) + 3S_{44}} \quad (V.6)$$

are the bulk modulus and shear modulus in terms of the elastic stiffness and compliance coefficients.

In the actual case, the elastic energy is

$$E = \frac{1}{2} m e^2$$

where  $m$  is some unknown longitudinal modulus. It has been proved that<sup>64</sup>

$$m_R \leq m \leq m_V.$$

Experiment has shown that  $m$  is very close to the arithmetic average of the Voigt and Ruess approximations;<sup>35</sup>

$$m \approx \frac{m_R + m_V}{2}. \quad (V.7)$$

Since

$$E_y = \frac{1}{2} m_y e^2$$

is the energy stored for uniform uniaxial strain and

$$E = \frac{1}{2} m e^2$$

is the actual energy stored, the difference,

$$\delta E = \frac{1}{2} (m_y - m) e^2,$$

is the energy stored in random strain. For simplicity, an upper bound for this random strain energy can be obtained by replacing  $m$  with  $m_R$ . Call this upper bound  $\overline{\delta E}$ . An upper bound for the ratio of random strain energy to uniform uniaxial strain energy is

$$\frac{\overline{\delta E}}{E_y} = \frac{m_y - m_R}{m_y}.$$

From Equation (V.1) through Equation (V.6), this is approximately

$$\frac{\overline{\delta E}}{E_y} = \frac{1}{\left(1 + \frac{3}{4} \frac{K}{\mu}\right)} \frac{(S - 1)^2}{\left(1 + \frac{2}{3} S\right) \left(1 + \frac{3}{2} S\right)} \quad (V.8)$$

where

$$S = \frac{2c_{44}}{c_{11} - c_{12}}$$

is a measure of the isotropy of the material. (This is exact for  $K$  and  $\mu$  replaced by  $K_y$  and  $\mu_y$  but the difference is negligible.)

Since the energy is proportional to the square of the strain, an upper bound measure of the ratio of the random strain to the uniform strain is

$$\frac{\bar{e}_{\text{(random)}}}{e_{\text{(uniform)}}} = \left[ \frac{1}{\left(1 + \frac{3}{4} \frac{K}{\mu}\right)} \frac{(S - 1)^2}{\left(1 + \frac{2}{3} S\right) \left(1 + \frac{3}{2} S\right)} \right]^{1/2}. \quad (\text{V.9})$$

For YIG,  $\mu = 0.78 \times 10^{12}$  dynes/cm<sup>2</sup>,  $K = 1.62 \times 10^{12}$  dynes/cm<sup>2</sup>, and  $S = 0.95$ . This gives

$$\frac{\bar{e}_{\text{(random)}}}{e_{\text{(uniform)}}} = 0.0015.$$

Copper is an example of a highly anisotropic cubic material.  $\mu = 0.436 \times 10^2$  dynes/cm<sup>2</sup>,  $K = 1.33$  dynes/cm<sup>2</sup>, and  $S = 3.2$ . For copper,

$$\frac{\bar{e}_{\text{(random)}}}{e_{\text{(uniform)}}} = 0.28.$$

It was stated that this was an upper bound. A better estimate can be made by using Equation (V.7) in the analysis. The result differs from Equation (V.9) by a factor of  $1/\sqrt{2}$ . This gives a strain ratio in copper of 0.20.

This calculation shows that the assumption of uniform strain in YIG is quite good. However, for highly anisotropic material the deviation from uniform strain can be quite appreciable.